Acta Pharmaceutica Sinica B 2024;14(3):1283−1301

Chinese Pharmaceutical Association
Institute of Materia Medica, Chinese Academy of Medical Sciences

Acta Pharmaceutica Sinica B

www.elsevier.com/locate/apsb
www.sciencedirect.com

ORIGINAL ARTICLE

Design and discovery of a highly potent ultralong-acting GLP-1 and glucagon co-agonist for attenuating renal fibrosis

Qian Zhao[a,†], Jiale Dong[a,†], Han Liu[a,†], Hui Chen[a], Huan Yu[a], Shuyin Ye[d], Shuangjin Yu[b], Yu Li[d], Longhui Qiu[b], Nazi Song[a], Hongjiao Xu[a], Qi Liu[d], Zhiteng Luo[a], Yuyi Li[c], Rui Wang[e,*], Guodong Chen[b,*], Xianxing Jiang[a,*]

[a]*School of Pharmaceutical Sciences, Guangdong Provincial Key Laboratory of Chiral Molecule and Drug Discovery, Sun Yat-sen University, Guangzhou 510006, China*
[b]*Organ Transplant Center, the First Affiliated Hospital, Sun Yat-sen University, Guangzhou 510006, China*
[c]*Zhongshan School of Medicine, Sun Yat-sen University, Guangzhou 510006, China*
[d]*Shenzhen Turier Biotech. Co., Ltd., Shenzhen 518118, China*
[e]*School of Life Sciences, Key Laboratory of Preclinical Study for New Drugs of Gansu Province, School of Basic Medical Sciences & Research Unit of Peptide Science, Chinese Academy of Medical Sciences, Lanzhou University, Lanzhou 730000, China*

Received 19 July 2023; received in revised form 9 October 2023; accepted 9 November 2023

KEY WORDS

GLP-1 receptor;
Glucagon receptor;
Chronic kidney disease;
Diabetic nephropathy;
Kidney fibrosis;
Dual-agonism

Abstract The role of co-agonists of glucagon-like peptide-1 receptor (GLP-1R) and glucagon receptor (GCGR) in chronic kidney disease (CKD) remains unclear. Herein we found that GLP-1R and GCGR expression levels were lower in the kidneys of mice with CKD compared to healthy mice and were correlated with disease severity. Interestingly, GLP-1R or GCGR knockdown aggravated the progression of kidney injury in both diabetic *db/db* mice and non-diabetic mice undergoing unilateral ureteral obstruction (UUO). Based on the importance of GLP-1R and GCGR in CKD, we reported a novel monomeric peptide, 1907-B, with dual-agonism on both GLP-1R and GCGR. The data confirmed that 1907-B had a longer half-life than long-acting semaglutide in rats or cynomolgus monkeys (∼2−3 fold) and exhibited better therapeutic contribution to CKD than best-in-class monoagonists, semaglutide, or glucagon, in *db/db* mice and UUO mice. Various lock-of-function models, including selective pharmacological

*Corresponding authors.
E-mail addresses: wangrui@lzu.edu.cn (Rui Wang), chguod@mail.sysu.edu.cn (Guodong Chen), jiangxx5@mail.sysu.edu.cn (Xianxing Jiang).
[†]These authors made equal contributions to this work.
Peer review under the responsibility of Chinese Pharmaceutical Association and Institute of Materia Medica, Chinese Academy of Medical Sciences.

https://doi.org/10.1016/j.apsb.2023.11.020

activation and genetic knockdown, confirmed that 1907-B's effects on ameliorating diabetic nephropathy in *db/db* mice, as well as inhibiting kidney fibrosis in UUO mice, were mediated through GLP-1 and glucagon signaling. These findings highlight that 1907-B, a novel GLP-1R and GCGR co-agonist, exerts multifactorial improvement in kidney injuries and is an effective and promising therapeutic option for CKD treatment.

1. Introduction

Chronic kidney disease (CKD), characterized by persisting kidney damage and impairment of kidney function, remains a major public health problem with high morbidity[1,2]. The end-stage kidney disease, which is a consequence of chronic kidney failure, is manifested by glomerulosclerosis, tubulointerstitial fibrosis, and vascular sclerosis[3,4]. Unfortunately, the molecular mechanisms linking pathogenetic factors to kidney fibrosis are complicated and poorly understood[5,6]. This process most likely involves oxidative stress[7−10], inflammation[11−13], epithelial-mesenchymal transition, apoptosis[14], and extracellular matrix deposition[15]. As of now, there is an urgent need for investigations to explore therapeutic targets and develop corresponding approaches for the treatment of CKD.

The mitochondrion is a fundamental organelle that regulates cellular redox and energy homeostasis, making it a major source of intracellular oxidative stress[16]. Emerging evidence suggests mitochondrial dysfunction and damage could be the primary factor causing various types of CKDs through impaired adenosine triphosphate (ATP) generation, increased mitochondrial DNA (mtDNA) damage, and the production of reactive oxygen species (ROS)[17−20]. Recent studies have demonstrated that ameliorating mitochondrial dysfunction can prevent the progression of kidney diseases[21−23]. Hence, mitochondria have been identified as an attractive target for drug development to restrain CKD progression.

The protective role of GLP-1R signaling in diabetic nephropathy is attributed to its hypoglycemic effect and anti-oxidative effect[24−28]. On the other hand, glucagon has been shown to improve mitochondrial turnover and function in various tissues, including the liver, heart, and muscle[29,30]. In summary, both GLP-1 and glucagon can potentially influence mitochondrial function, albeit through different mechanisms. Moreover, the potential for GLP-1 agonism to counteract hyperglycemia could mitigate the risk of excessive glucagon agonism leading to diabetes. Combining the lipolytic and thermogenic effects associated with glucagon, alongside the appetite-suppressing effects of GLP-1, offers a compelling mechanistic basis for the creation of a synergistic co-agonist peptide[31]. At present, the application of GLP-1R/GCGR dual-target agonists in nonalcoholic steatohepatitis (NASH)[32,33], obesity[34−37], and diabetes[38,39] has attracted extensive attention. The relevant drugs in clinical trials include Cotadutide (MEDI0382)[40], HM-12525A[41], Oxyntomodulin (OPK-88003, TT401), and BI456906. However, the therapeutic effects of these co-agonists on kidney fibrosis remain unknown.

In this study, we first showed that kidney GLP-1R and GCGR expression levels were lower in CKD mice than in healthy mice and were correlated with disease severity. Interestingly, kidney-specific knockdown of GLP-1R and GCGR aggravated the progression of kidney injury in both diabetic *db/db* mice and non-diabetic mice with UUO. Differing from prior research that focused solely on the role of GLP-1R in CKD, we discovered that GCGR also played a key role in the progression of CKD. These findings led us to develop a highly potent GLP-1R/GCGR co-agonist as a treatment for CKD. Here, we originally introduced the concept of "double-site recognition" *via* octadecanedioic (C18) and the glycine/serine-based linker (GGSGSG) binding to albumin to optimize drug release. Finally, we successfully developed 1907-B, an ultralong-acting GLP-1R/GCGR dual-target agonist that has an anti-oxidative impact and can boost mitochondrial turnover. Preclinical studies demonstrated that 1907-B could significantly ameliorate kidney fibrosis. This promising alternative therapy for CKD is currently undergoing Phase I clinical trials.

2. Methods

2.1. Synthesis of peptides

According to the standard protocol of solid-phase peptide synthesis (SPSS), a series of dual glucagon-like peptide 1/glucagon receptor agonists (1901−1917 and 1907-B) were synthesized using 4-methylbenzhy-drylamine (MBHA) resin (GL Biochem, Shanghai, China). Reversed-phase high-performance liquid chromatography-mass spectrometric (RP-HPLC-MS, Agilent Technologies, USA) was used to perform the peptide purification and atomic accumulation process. The analysis results are shown in Supporting Information Figs. S10−S11. The GLP-1R agonists (liraglutide and semaglutide) and GCGR agonist (glucagon) were ordered from Hybio Pharmaceutical Co., Ltd.

2.2. Circular dichroism (CD) measurements

The CD measurements of the series of dual glucagon-like peptide 1/glucagon receptor agonists were performed by the Chirascan CD spectrometer in a 2 mm pathlength cuvette at 25 °C. The spectra were recorded from 190 to 260 nm and averaged over 3 scans with a resolution of 0.5 nm, a bandwidth of 1.0 nm and a response time of 3 s. All peptides were dissolved to 40 μmol/L in PBS or 50% TFE. The mean residue ellipticity was plotted *vs* wavelength.

2.3. Generation of CRE-Luc stable cell line over-expressing GLP-1R or GCGR

HEK-293 cell line was obtained from the Type Culture Collection of the Chinese Academy of Sciences (Shanghai, China). The cell was cultured in DMEM with 10% FBS and 1% penicillin-

streptomycin (Gibco, Thermo Fisher Scientific, USA) in a humidified atmosphere with 5% CO_2 at 37 °C. Lentivirus encoding firefly luciferase gene under the control of cAMP-responsive element (CRE) promoter was used to establish the CRE-Luc stable HEK-293 cell line. After being exposed to the complete medium containing 1 μg/mL puromycin for 1 week, the surviving cells (CRE-HEK293) were amplified and then transfected with a G418 selective mammalian expression plasmid which encoded Renilla luciferase gene under the control of human GLP-1R or GCGR. Single colony stable cell line over-expressing both CRE-firefly luciferase and GLP-1R- or GCGR-Renilla luciferase (GLP-1R- or GCGR-CRE-HEK293) was then generated for GLP-1R or GCGR activation reporter assay *in vitro*.

2.4. GLP-1R or GCGR activation reporter assay in vitro

GLP-1R- or GCGR-CRE-HEK293 cells were seeded in 96-well plates at a density of 4×10^4 cells per well and cultured for 36 h in DMEM containing 10% FBS and 1% penicillin−streptomycin. After starving for 6 h, GLP-1R- or GCGR-CRE-HEK293 cells were treated with peptides in a series of doses for 5 h. The GLP-1R or GCGR activation was assessed by the ratio of firefly luminescence intensities to Renilla luminescence intensities, using Dual-Luciferase Reporter Gene Assay Kit (Yeasen, Shanghai, China) following the manufacturer's instruction. The data were fit by GraphPad Prism 9.0 software (GraphPad, San Diego, CA, USA) to calculate the EC_{50} of each peptide.

2.5. Cell culture and treatment

The mouse tubular epithelial cells (mTEC) and glomerular mesangial cells (GMC) were kindly provided by Professor Wang from Lanzhou University. Both mTEC cells and GMC cells were cultured in low-glucose DMEM (Gibco, Thermo Fisher Scientific, USA) with 10% FBS and 1% penicillin−streptomycin. Cells were plated on 6-well plates and cultured for 24 h. After serum-free overnight, cells were exposed to high glucose or 10 ng/mL TGF-β and meanwhile treated with 20.0 μmol/L peptides for 48 h. In indicated experiments, cells were administrated with PKA inhibitor, H89 (5.0 μmol/L) (Beyotime Biotechnology, China).

2.6. Animal model and sample collection

Mice in all studies were healthy and immune-normal and kept in a 12 h light−dark cycle in the specific-pathogen-free (SPF) environment, permitting access to food and water freely. All the protocols of animal research conformed to the U.S. Public Health Service Policy on Use of Laboratory Animals and were approved by the Ethics Committee on Use and Care of Animals of Sun Yat-sen University.

For the diabetic nephropathy (DN) model, eight-week-old male Lepr *db/db* (*db/db*) and Lepr *db/m* (*db/m*) mice in a C57BLKS/J background were purchased from the GemPharmatech™. To assess the pharmacological effects of 1907-B, DN mice were administrated with semaglutide (120.0 μg/kg/day), glucagon (120.0 μg/kg/day) or 1907-B (60.0, 120.0 and 240.0 μg/kg/day or 120.0 μg/kg/2 days) for 8 weeks ($n = 6$ for per group; subcutaneous injection). The fasting blood glucose and body weight of DN mice were recorded every two days.

For the UUO model, eight-week-old male C57BL/6J mice were obtained to establish the UUO model following a standard protocol. After being administrated with 5% chloral hydrate, mice were incised dorsally to expose the left ureter near the renal pelvis. Then the complete unilateral ureteral obstruction was performed in the left ureter by double-ligating using 6-0 nylon. The ureters of mice in the sham-operated group were exposed, but not ligated. To evaluate the effects of 1907-B, UUO mice were administrated with semaglutide (120.0 μg/kg/day), glucagon (120.0 μg/kg/day) or 1907-B (60.0, 120.0 and 240.0 μg/kg/day or 120.0 μg/kg/2 days) for 14 days ($n = 6$ for per group; intraperitoneal injection). Kidneys were harvested 14 days after UUO surgery.

For the Zucker Diabetic Fatty (ZDF) model, 1907-B was administered subcutaneously at doses of 30.0, 100.0, and 300.0 μg/kg every other day for 18 weeks. Semaglutide was used as a positive control for comparison. The effects of 1907-B on blood sugar, glycosylated hemoglobin, urine kidney function, kidney pathology, blood lipids, liver function, body weight and other improvement effects were further evaluated.

Prior to the sacrifice at the study terminal, all mice were fasted overnight and anesthetized with 5% chloral hydrate. Blood samples were collected from the posterior venous plexus of the eyes, and were separated to obtain serum by centrifugation at $1000 \times g$ for 15 min. The serum was stored at −80 °C for further biochemical assays. Kidney tissue, liver tissue and epididymal adipose tissue were collected and frozen in liquid nitrogen immediately, and then stored at −80 °C or fixed in 10% paraformaldehyde for histological assessment.

2.7. The pharmacokinetic parameters of semaglutide and 1907-B in rats

Twenty-four SD rats (12 male and 12 female) were randomly divided into four groups: SC-semaglutide, SC-1907-B, IV-semaglutide and IV-1907-B. SC-semaglutide and SC-1907-B were treated with 0.05 mg/kg semaglutide and 1907-B by subcutaneous injection, respectively. Blood samples were collected at 0 min (before peptides administration) and 10, 20, 30 min, 1, 2, 4, 6, 8, 24, 36, 48, 72 h, 4, 5, 6 and 7 day after peptides administration. IV-semaglutide and IV-1907-B were given 0.05 mg/kg semaglutide and 1907-B *via* tail vein, respectively. Blood samples were collected at 0 min (before peptides administration) and 10, 20, 30 min, 1, 2, 4, 6, 8, 24, 36, 48, 72 h, 4, 5, 6 and 7 day after peptides administration. The concentrations of semaglutide and 1907-B in plasma were determined by the developed LC−MS/MS method. The pharmacokinetic parameters were calculated by the non-compartment model using WinNonlin 6.4.

2.8. The pharmacokinetic parameters of 1907-B in cynomolgus monkeys

The pharmacokinetic study was performed in Covance (Shanghai, China). Cynomolgus monkeys of either sex ($n = 2$) were given an intravenous (i.v.) dose of 25.0 μg/kg and subcutaneous (s.c.) dose of 25.0 μg/kg. Serial blood samples were collected for the determination of plasma 1907-B concentrations using a validated HPLC−MS/MS method. Pharmacokinetic analysis was carried out using non-compartmental procedures with Phoenix WinNonlin (version 8.1).

2.9. AAV9-RNAi mediated GLP-1R and GCGR knockdown

The custom-made adeno-associated virus (AAV) serotype 9 carrying shRNA for mouse GLP-1R (AAV9-GLP-1R-shRNA), shRNA for mouse GCGR (AAV9-GCGR-shRNA), and mouse nonsense control shRNA (AAV9-Control-shRNA) were purchased from Genechem (Shanghai, China). The adeno-associated virus was injected into mice (10^{11} v.g., *via* subcapsular injection into the parenchyma of the kidney and tail vein injection in *db/db* mice, and retrograde infusion into the renal vein in UUO mice) to knock down GLP-1R and GCGR, respectively. Target sequences are listed in Supporting Information Table S3.

Four weeks after administration with AAV9-RNAi to knock down *GLP-1R* or *GCGR*, *GLP-1R*$^{-/-}$ or *GCGR*$^{-/-}$ *db/db* mice were treated with semaglutide (120.0 μg/kg/day), glucagon (120.0 μg/kg/day) and 1907-B (120.0 μg/kg/2 days) for 8 weeks to evaluate the pharmacological effects of 1907-B ($n = 6$ for per group; subcutaneous injection). Fasting blood glucose and body weight were measured every two days.

Three weeks after administration with AAV9-RNAi to knock down *GLP-1R* or *GCGR*, *GLP-1R*$^{-/-}$ or *GCGR*$^{-/-}$ C57BL/6J mice were used to establish the UUO model, as above described. To assess the pharmacological effects of 1907-B, GLP-1R$^{-/-}$ or GCGR$^{-/-}$ UUO mice were treated with semaglutide (120.0 μg/kg/day), glucagon (120.0 μg/kg/day) and 1907-B (120.0 μg/kg/2 days) for 14 days ($n = 6$ for per group; daily intraperitoneal injection). Kidneys were harvested 14 days after UUO surgery.

2.10. Fasting blood glucose measure, OGTT and ITT

Fasting blood glucose was evaluated utilizing blood from tail nicks by OneTouch UltraVue Blood Glucose Metet and test strips (Johnson & Johnson, USA). After being administrated with semaglutide, glucagon, 1907, 1917 or 1907-B, all mice fasted for 6 h and were performed fasting blood glucose assays.

For OGTT, KM or *db/db* mice were treated with 1901−1917 or 1907-B for the indicated time. After fasting overnight, glucose solution (0.5 g/mL, Tianjin Zhiyuan Reagent Co., Ltd., China) was orally injected into mice (2 g/kg of body weight). Blood glucose level was recorded at baseline, 15, 30, 60, 90 and 120 min.

One week after the OGTT assay, ITT in *db/db* mice was performed. After fasting for 6 h, *db/db* mice were injected intraperitoneally with 0.25 U/kg insulin (Novolin R, Denmark). Blood glucose level was assessed at 15, 30, 60 and 90 min.

2.11. Biochemical assays

The levels of serum creatinine, blood urea nitrogen, 24 h-albuminuria, urine glucose, serum ALT, serum AST, serum TC and serum TG were determined using the corresponding assay kits (Nanjing Jiancheng Bioengineering Institute, China). The levels of insulin in *db/db* mice serum were examined utilizing relative ELISA kits (Cloud-Clone Corp, China) referring to the protocols. The Hemoglobin A1c (HbA1c) levels in the serum of *db/db* mice were measured using A1CNow®+ following the manufacturer's instructions (Sinocare, China). The levels of GSH and the activities of CAT and SOD in the kidneys of *db/db* mice were assessed according to the standard protocols provided by the manufacturer (Nanjing Jiancheng Bioengineering Institute, China).

2.12. Surface plasmon resonance assay

SPR assays were used to assess the peptides 1907 and 1907-B binding affinities of human serum albumin (HSA) *via* Biacore 8K, a high-sensitivity SPR system (Cytiva, UK). Following the standard amine coupling protocol, HSA was overlaid on the sensor. 1907 or 1907-B was dissolved respectively to a series of concentrations in running buffer (PBS, pH = 7.4, Sigma−Aldrich Ltd., Merck, Germany). Samples were permitted to flow through the chip surface at the flow rate of 25 μL/min. After each injection cycle, the surface was injected 25 μL of 10 mmol/L NaOH (Sigma−Aldrich Ltd., Merck, Germany) twice for regeneration. The data were fit by Biacore 8K analysis software (Cytiva) to calculate the binding constants of 1907 or 1907-B.

2.13. Isothermal titration calorimetry

ITC assays were performed on MicroCal PEAQ-ITC System (Malvern Instruments Ltd.) in PBS (pH = 7.4) at 37 °C. In all experiments, 1907, 1907-B or GGSGSG was in the syringe and human serum albumin was in the sample cell. The data were analyzed using MicroCal PEAQ-ITC Analysis Software. Heats of dilution were assessed using the final injections of each individual titration and subtracted before data analysis.

2.14. Mitochondrial oxygen consumption

The evaluation of mitochondrial oxygen consumption was performed using the Seahorse Xfe96 Analyzer (Agilent). The mTEC cells or GMC cells were plated at a density of 5000 cells per well and were administrated as mentioned above. Prior to being placed in the Seahorse Xfe96 Analyzer, the plate was placed in a CO_2-free incubator for 30 min. 1 μmol/L oligomycin (Agilent), 0.5 μmol/L FCCP (Agilent) and 5 μmol/L antimycin A (Agilent) were used in the mitochondrial stress test according to the standard protocols. The OCRs were normalized to the protein mass.

2.15. Histological examination

Formalin-fixed kidney tissues embedded in paraffin were sectioned into 5 μm slices. After deparaffinization and rehydration, the Hematoxylin and Eosin (H&E), Sirius Red staining and Masson staining for collagen and Periodic Acid-Schiff for glycogen accumulation were performed in section slices, referring to the standard protocols, respectively.

2.16. Immunohistochemistry staining

For immunofluorescent staining, after deparaffinization and rehydration, antigen retrieval was carried out by heating section slices in 10 mmol/L sodium citrate buffer (pH = 6.0) for 15 min. The section slices were then incubated with 3% hydrogen peroxide for 10 min to eliminate the endogenous peroxidase activity. Next, section slices were blocked with 1% BSA solution for 1 h at room temperature and then were incubated with primary antibodies at 4 °C overnight following secondary antibodies for 1 h. After being administrated with DAB, hematoxylin staining was performed in the section slices. The antibodies used for immunohistochemistry staining are described in Supporting Information Table S4.

2.17. Immunofluorescent staining

For immunofluorescent staining, after deparaffinization and rehydration, antigen retrieval was carried out by heating section slices in 10 mmol/L sodium citrate buffer (pH = 6.0) for 15 min. Next, section slices were blocked with 1% BSA solution for 1 h at room temperature and then were incubated with primary antibodies at 4 °C overnight following secondary antibodies for 1 h. The nucleus was counterstained with DAPI. The staining was viewed and photographed under confocal microscopy. The antibodies used for immunofluorescent staining are described in Table S4.

2.18. Protein isolation and Western blotting

Total protein extracts from mTEC cells, GMC cells or kidney tissues using RIPA (Beyotime Biotechnology, China). The concentration of protein was assessed by the BCA Kit (Pierce, ThermoFisher Scientific, USA). Thirty micrograms of protein were separated by 10% or 12% sodium dodecyl sulfate-polyacrylamide gel electrophoresis depending on the band of the target protein. Next, the proteins in the gel were transferred onto an equilibrated polyvinylidene difluoride membrane (PVDF, Immobilon®-PSQ transfer membranes, Merck Millipore, Germany). Membranes were blocked by 5% skim milk and then interacted overnight with primary antibodies at 4 °C, following HRP-labeled secondary antibodies at room temperature for 1 h. The blots were detected by enhanced chemiluminescence (Glarity™ Western ECL Substrate, Bio-Rad, USA) and the signals were recorded and quantified *via* Tanon-Image Software (Shanghai, China). Data normalization was performed using reference antibody GAPDH or β-actin. The antibodies used for Western blotting are described in Supporting Information Table S4.

2.19. RNA isolation and quantitative real-time polymerase chain reaction

Total RNA was isolated and purified using TRIZOL Reagent (Invitrogen, MA, USA) from kidney tissues, following the manufacturer's instructions. The concentration of RNA was assessed by Nanodrop 2000 (ThermoFisher Scientific, USA). First Strand cDNA synthesis Super Mix (TransGen Biotech, China) was used to reverse transcribe 4 μg of total RNA into cDNA. Quantitative real-time PCR (qRT-PCR) was performed in the Light Cycler 480 Real-Time PCR System (Roche, Swiss) using SYBR Green qPCR Super Mix (TransGen Biotech, China). The *C*p values were calculated and the data were normalized to the housekeeping expression (β-actin). Primer sequences are described in Supporting Information Table S5.

2.20. RNA sequencing

The isolation and prurition of total RNA from kidney tissues were performed as mentioned above. RNA libraries were sequenced on the Illumina sequencing platform by LC-BIO Co., Ltd. (Hangzhou, China).

2.21. Gene set enrichment analysis

Gene Set Enrichment Analysis (GSEA) was performed using the OmicShare tools, a free online platform for data analysis (http://www.omicshare.com/tools). For each KEGG biological pathway, involved genes were defined as a gene set, and then a ranked list and a 'gene set' permutation type of the gene set were constructed. Gene sets with $|NES| > 1$, NOM P-values < 0.05 and FDR q-values < 0.25 were considered statistically significant.

2.22. Drug target profile screening of 1907-B

Methods employed in this study have been adapted from the scientific literature to maximize reliability and reproducibility. Reference standards were run as an integral part of each assay to ensure the validity of the results obtained. Assays were performed by Shenzhen Turier Biotech Co., Ltd.

2.23. Quantification and statistical analysis

The positive area of stained slices was quantified by ImageJ (https://imagej.nih.gov/ij/). All data in this study were shown as the mean ± SD (Standard Deviation). GraphPad Prism 9.0 software (https://www.graphpad.com/) was used to determine the statistical significance. The differences were assessed using Student's t-test or one-way analysis of variance (ANOVA), and significance was considered when $P < 0.05$.

3. Result

3.1. The expression levels of GLP-1R and GCGR are associated with CKD

We first detected the gene expression levels of GLP-1R and GCGR in kidney samples from healthy mice or mice with CKD. The decreased protein expression levels of GLP-1R and GCGR in kidneys were found in two mouse models of CKD, including db/db mice, a diabetic nephropathy (DN) mouse model, and UUO mice, a non-diabetic kidney fibrosis mouse model (Fig. 1A). Furthermore, qPCR results also confirmed that Glp1r and Gcgr mRNA expression levels were decreased in the kidneys of *db/db* mice and UUO mice than in those of the control group (Fig. 1B). Collectively, the marked down-regulation of GLP-1R and GCGR levels observed in mouse models indicated that the GLP-1R and GCGR signaling plays critical roles in CKD progression.

To define the importance of GLP-1R and GCGR in CKD, we utilized AAV9 to transduce GLP-1R or GCGR shRNA and delivered them to kidneys as an approach to down-regulate GLP-1R and GCGR expression in mice[42,43]. Considering the high post-surgical mortality in diabetic mice, we performed three different injection strategies, including subcapsular injection into the parenchyma of the kidney and tail vein injection in *db/db* mice, and retrograde infusion into the renal vein in UUO mice, as shown in Fig. 1C. All of these approaches could successfully down-regulate GLP-1R and GCGR expression levels in the kidney. We found that GLP-1R and GCGR knockdown aggravated CKD in both *db/db* mice and UUO mice (Fig. 1D and Supporting Information Fig. S1). The RNA sequencing data also suggested a significant increase expression of genes related to fibrotic factors and inflammation and an obvious decrease expression of genes related to mitochondrial function (Fig. 1E and F). Thus, our findings demonstrated that GLP-1R and GCGR are key regulators of chronic kidney injury and could be potential therapeutic targets of CKD.

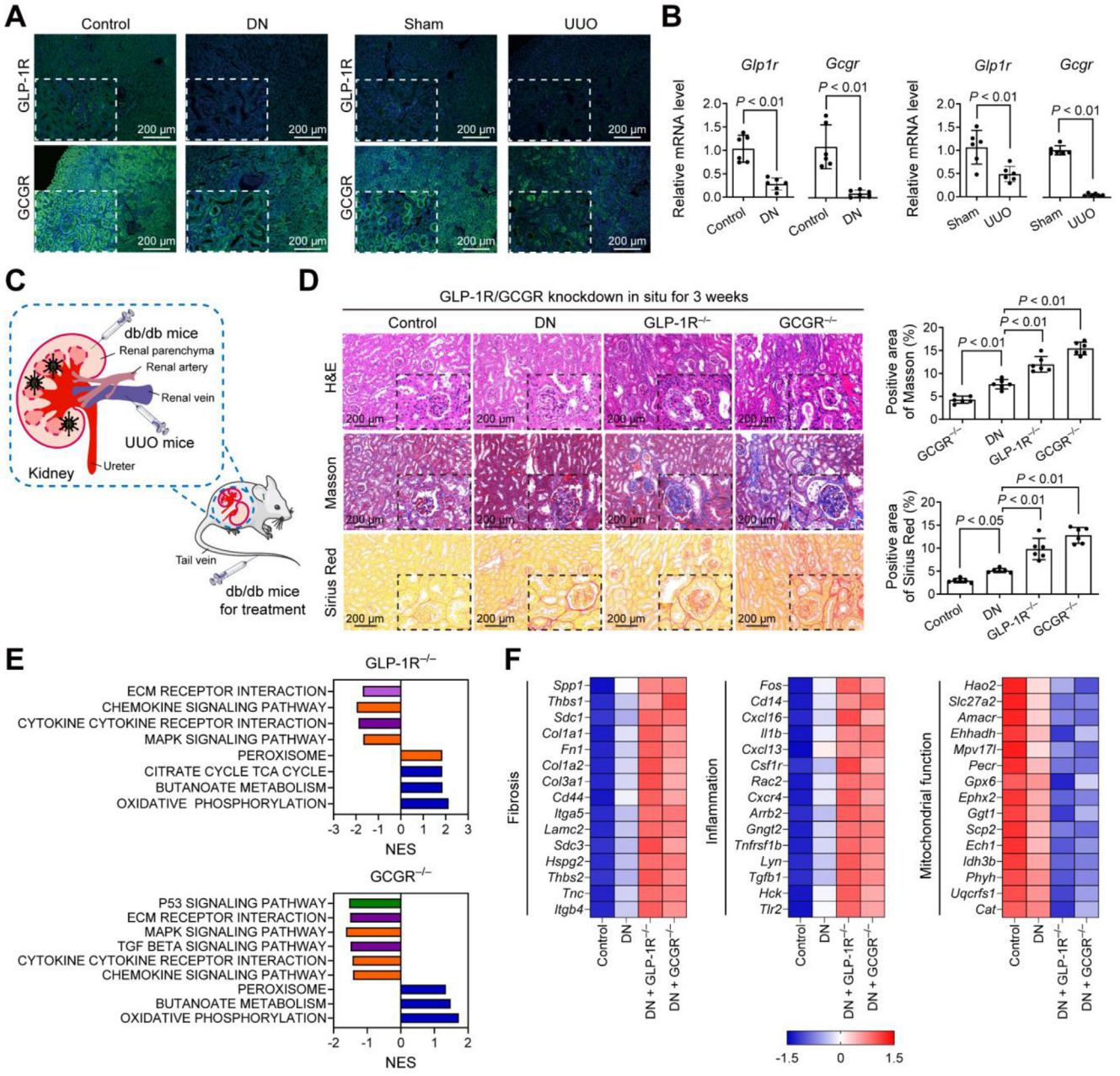

Figure 1 GLP-1R and GCGR expression is correlated with chronic kidney disease (CKD) in mice. (A) GLP-1R and GCGR immunofluorescence staining of kidneys from diabetic *db/db* mice ($n = 6$) or UUO mice ($n = 6$). (B) The mRNA levels of *Glp1r* and *Gcgr* in kidneys from diabetic *db/db* mice ($n = 6$) and UUO mice ($n = 6$). (C) Experimental scheme for generating of GLP-1R and GCGR knockdown mice *via* different injection. (D) Representative images of H&E, Masson, and Sirius Red in kidneys from diabetic *db/db* mice after AAV9-CON, AAV9-GLP1R-RNAi, or AAV9-GCGR-RNAi treatment for 3 weeks. (E) GSEA of pathways related to fibrosis, inflammation, and mitochondrial function in diabetic *db/db* mice treated with AAV9-CON, AAV9-GLP1R-RNAi, or AAV9-GCGR-RNAi ($n = 6$/group). (F) Heatmap of fibrosis-, inflammation-, and mitochondrial function-related gene expression profiles based on the RNA-Seq dataset. Here and hereafter, unless otherwise indicated, three separate experiments were performed for each assay ($n = 3$ samples/group or $n = 3-6$ mice/group for each experiment). All the above data are presented as mean values ± SD using the unpaired Student's *t*-test. Source data are provided as a Source Data file.

3.2. The design of GLP-1R and GCGR dual-agonists and related structure−activity relationship research

Based on the above results, combining the activity of GLP-1 and glucagon with complementary biological effects may offer a favorable strategy to treat diabetic nephropathy and related CKD. We therefore created 17 novel GLP-1/glucagon chimeric peptides 1901−1917 by fusing key amino acid sequences responsible for maintaining the biological activity of GLP-1 and glucagon (Fig. 2A)[44]. Glucagon achieves selectivity to GCGR through its C-terminal acid; thus, to reduce the specificity for GCGR and activate GLP-1R more effectively, these chimeric peptides were designed to end with a C-terminal amide[31]. Besides, the C-terminal decapeptide from exendin-4 was assembled in the

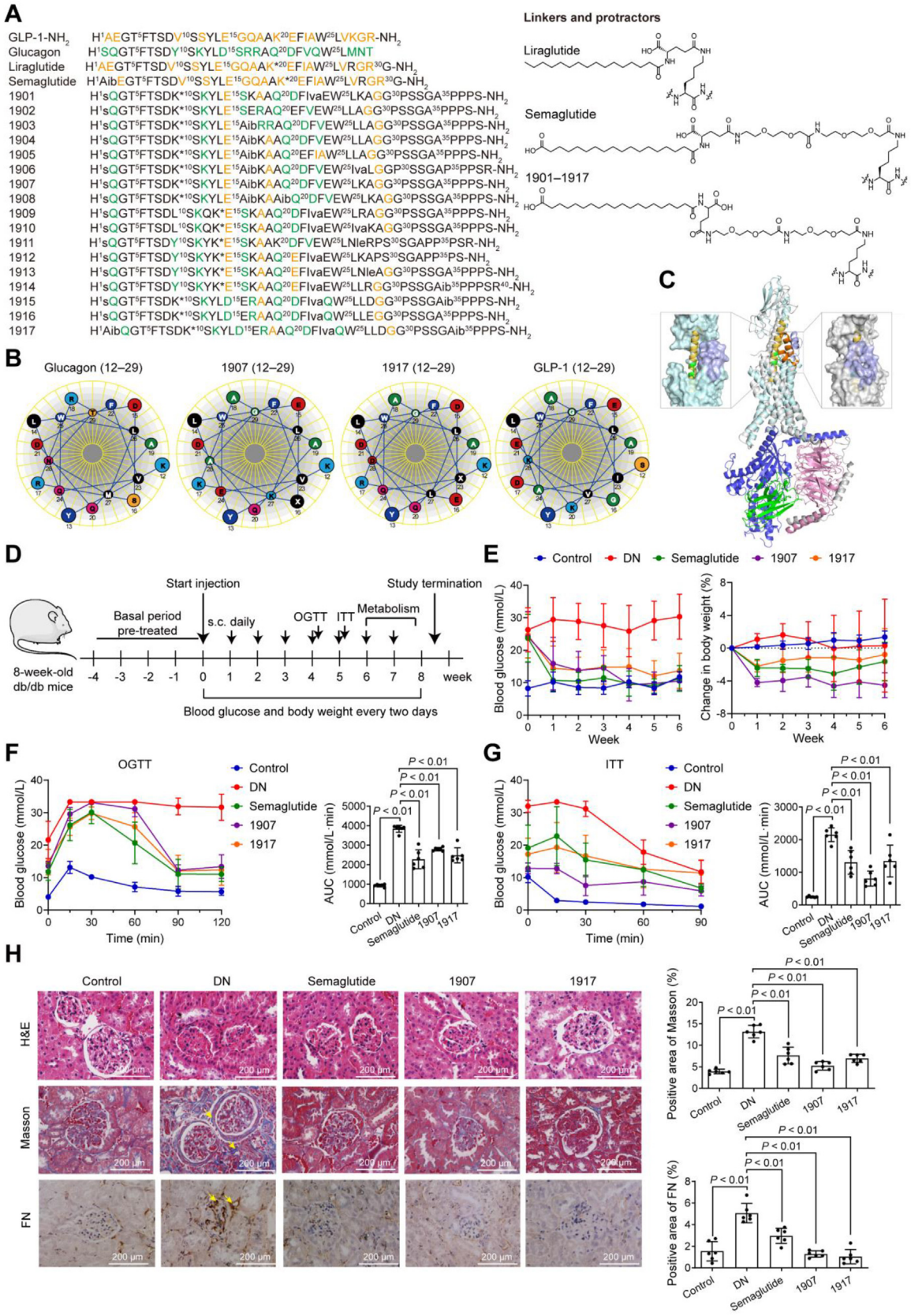

Figure 2 1907 and 1917 generate synergistic metabolic benefits and ameliorate CKD in diabetic *db/db* mice. (A) Sequence information of GLP-1, glucagon, liraglutide, semaglutide and 1901−1917. (B) Helical wheel representation of GLP-1, glucagon, 1907, and 1917. (C) Three-dimensional model of 1907/GLP-1R (PDB ID: 7LCJ). (D) Schematic of experimental procedures testing the pharmacological effects of 1907 and 1917 on diabetic *db/db* mice. (E) The fasting blood glucose and body weight change of diabetic *db/db* mice after 8-week administration with

C-terminus of chimeric peptides to further enhance GLP-1R efficacy[45]. It has been identified that the salt bridges formed between 16−20 or 17−21 with specific helix-favoring amino acids in pairs could enhance helix stability through constrained conformation (Fig. 2B)[46]. Considering that GLP-1 and glucagon commonly recognize their individual receptors through the α-helical conformation, we performed the amino acid substitutions in the middle of the peptides to stabilize the secondary structure and enhance binding affinities to related receptors. Based on the three-dimensional model of the 1907/GLP-1R complex by homologous modeling (Fig. 2C), we speculated that the introduction of the fatty acid side chain at residue 10 or 14 of these chimeric peptides would probably not perturb receptor binding interaction[44]. Therefore, these two residues were used as modification sites for the side chain to improve water solubility and prolong the half-life of peptide analogs[47].

Next, the structural conformation of these peptides was examined. As revealed in Supporting Information Fig. S2, these peptides showed the typical α-helical spectra in 50% TFE solution. We also found that the formation of salt bridges between 16−20 or 17−21 in these peptides was consistent with the helical content of these peptides (Supporting Information Table S1). Moreover, the agonistic activities among these peptide analogs were determined in HEK293 cells stably expressing human GLP-1R or GCGR using a cAMP response element (CRE)-driven luciferase reporter (Supporting Information Table S2). Liraglutide, as a positive control of GLP-1R agonist, activated GLP-1R half maximally at an effective concentration (EC_{50}) of 0.004 nmol/L and activated GCGR with an EC_{50} exceeding 1 μmol/L. Native glucagon activated GCGR at an EC_{50} of 0.010 nmol/L and activated GLP-1R with an EC_{50} exceeding 1 μmol/L. Other chimeric peptides also showed excellent GLP-1R agonism with the EC_{50} of 0.002−17.856 nmol/L. Meanwhile, the incorporation of glucagon residues gives part of chimeric peptides the ability to activate GCGR with the EC_{50} of 10.67−974.68 nmol/L.

Moreover, we performed the oral glucose tolerance test (OGTT) *in vivo* at different time points after peptide treatment to assess peptides' response to glucose and their long-acting potency. Liraglutide and semaglutide, known to have long half-lives, were used as positive controls. Blood glucose levels of mice treated with these peptides were significantly lower than those of control mice treated with PBS (Supporting Information Fig. S3A and S3B). Among them, the glucose-modulating effects of 1907 and 1917 were more significant than that of other peptide analogs, similar to semaglutide, and better than liraglutide (Fig. S3C). These data suggested that 1907 and 1917 had relatively prolonged half-lives and could be used to further evaluate the therapeutic effect on CKD *in vivo*.

3.3. *1907 and 1917 generate synergistic metabolic benefits and ameliorate kidney injury in* db/db *mice*

The *db/db* mice were chosen in the present study because they could spontaneously develop detectable DN[48]. 12-week-old male *db/db* mice were treated with 1907, 1917, or semaglutide for 8 weeks (Fig. 2D and Supporting Information Fig. S4), while db/m mice served as the nondiabetic controls. After 8 weeks of treatments, compared to those of the 20-week-old *db/db* mice, 1907, 1917 and semaglutide-treated *db/db* mice showed markedly reduced ballooning, hepatic steatosis, and liver weight, as well as lower serum lipid, including total cholesterol (TC) and triglyceride (TG) (Supporting Information Fig. S5). It should be noted that only 1907 treatment significantly decreased the body weight, which may be due to the distinct reduction in epididymis fat weight compared to other *db/db* mice (Fig. 2E and Fig. S5B). Collectively, these data suggested that 1907 treatment promoted lipid metabolism benefits and protected mice against lipid dysfunction.

The *db/db* mice exhibited higher fasting blood glucose levels compared to the control (db/m mice) during the 8-week experiment (as shown in Fig. 2E), whereas a noticeable decrease in the fasting blood glucose was observed in 1907, 1917 and semaglutide-treated *db/db* mice. In addition, 1907, 1917 and semaglutide treatment significantly reduced hyperglycemia-induced glucose intolerance and insulin resistance, as assessed by OGTT and insulin tolerance test (ITT); among them, 1907 worked best at improving insulin resistance (Fig. 2F and G). Furthermore, compared with db/m mice, *db/db* mice affected the islet topography, the number of insulins$^+$ cells and plasma insulin level. However, 1907, 1917 and semaglutide treatment could significantly improve islet cell numbers and promote the secretion of insulin (Supporting Information Fig. S6A and B). These data suggested that 1907, 1917 and semaglutide promoted glucose metabolism benefits and protected islets against the damage from hyperglycemia.

The kidney histopathology analysis was performed and the results indicated that the *db/db* mice displayed kidney damage and severe inflammatory infiltration (Fig. S6C and Fig. 2H), while administration of 1907, 1917, or semaglutide resulted in a marked decrease in kidney injury as determined by H&E and PAS staining. Moreover, the accumulation of collagen fibers was also reduced in 1907, 1917, or semaglutide treatment groups compared to the *db/db* mice (Fig. 2H and Fig. S6D). Taken together, these observations indicated that 1907, 1917, and semaglutide could decrease collagen deposition, thereby ameliorating kidney fibrosis.

3.4. *A rationally designed 1907 analog, 1907-B, exhibits balanced GLP-1R/GCGR potency and extended half-life*

Based on the above data, the analog 1907 was finally chosen for further modification to obtain a highly potent ultralong-acting GLP-1R and GCGR co-agonist with sufficient bioavailability. Because of the weak affinity between 1907 and GCGR, the C-terminal amide bond of 1907 was replaced with a C-terminal acid (Fig. 3A). We found that the 6-amino acid linker "GGSGSG" could bind to the HSA (K_D = 805 μmol/L), whereas tetraethylene glycol showed no HSA binding *via* isothermal titration calorimetry (ITC) assay (Fig. 3D). Thus, we hypothesized that strong and reversible binding to albumin by the combination of C18 and "GGSGSG" in the side chain of Lys at position 10 of 1907 (as 1907-B) would mediate increased stability toward proteolysis (Fig. 3B). Next, 1907 or 1907-B binding to HSA was evaluated in

semaglutide (120.0 μg/kg/day, n = 6), 1907 (120.0 μg/kg/day, n = 6) or 1917 (120.0 μg/kg/day, n = 6). (F−G) Oral glucose tolerance test (OGTT) and insulin tolerance test (ITT) were performed at the 4th or 5th week of semaglutide (120.0 μg/kg/day, n = 6), 1907 (120.0 μg/kg/day, n = 6) or 1917 (120.0 μg/kg/day, n = 6) administration. The corresponding area under curves (AUC) of blood glucose levels was calculated. (H) Representative images of H&E, Masson, and fibronectin (FN) staining in kidneys from diabetic *db/db* mice at indicated groups (n = 6/group) and bar graphs of positive area, respectively. Arrows indicate positive staining.

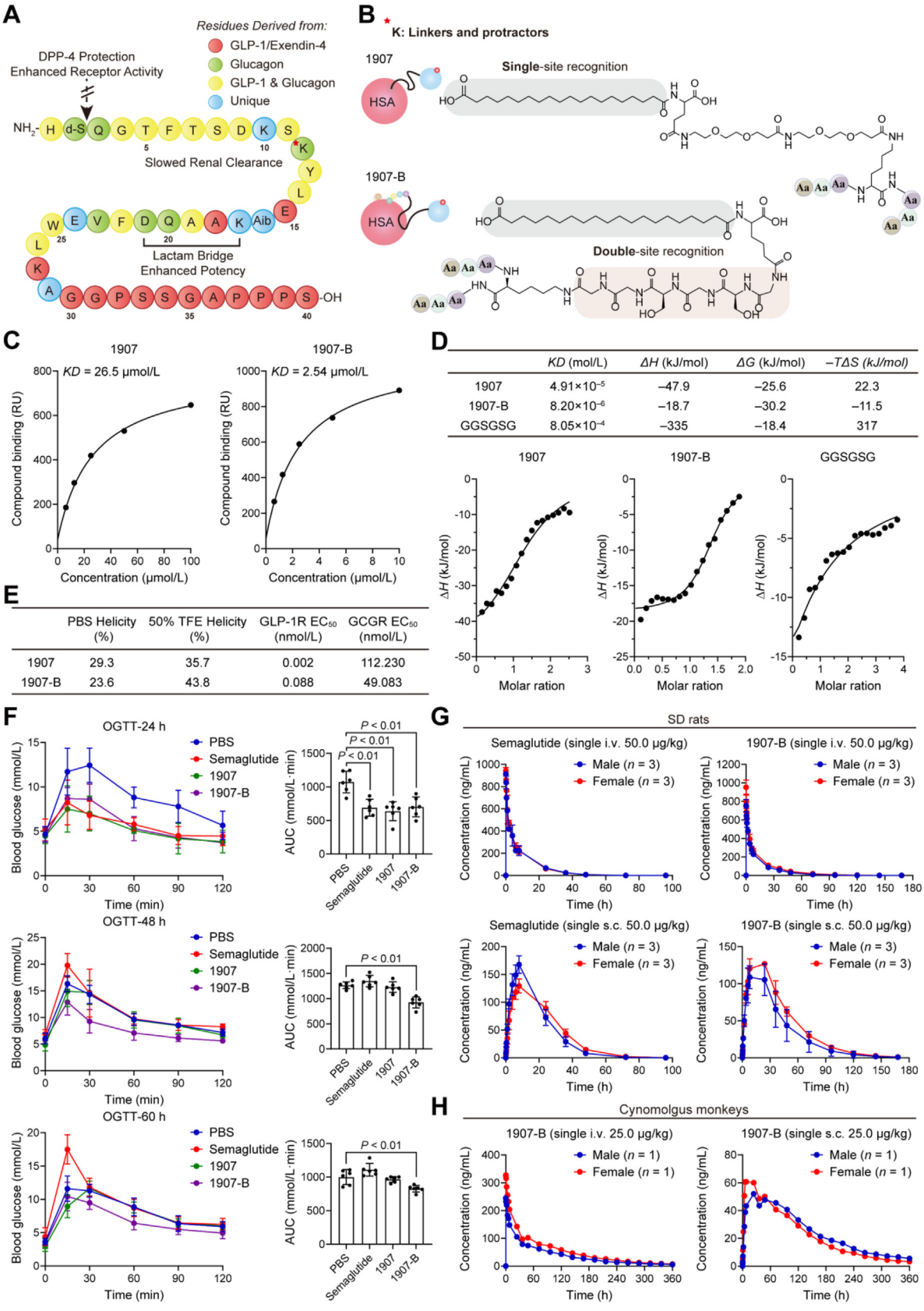

	KD (mol/L)	ΔH (kJ/mol)	ΔG (kJ/mol)	−TΔS (kJ/mol)
1907	4.91×10^{-5}	−47.9	−25.6	22.3
1907-B	8.20×10^{-6}	−18.7	−30.2	−11.5
GGSGSG	8.05×10^{-4}	−335	−18.4	317

	PBS Helicity (%)	50% TFE Helicity (%)	GLP-1R EC_{50} (nmol/L)	GCGR EC_{50} (nmol/L)
1907	29.3	35.7	0.002	112.230
1907-B	23.6	43.8	0.088	49.083

Figure 3 A rationally designed 1907 analog, 1907-B, exhibits an extended half-life *in vivo*. (A) The modification strategy to extend the half-life of 1907-B. (B) Chemical structures of the linkers and protractors of 1907 and 1907-B. (C) Surface plasmon resonance (SPR) sensorgrams showing binding of 1907 and 1907-B to human serum albumin. (D) Representative thermograms from isothermal titration calorimetry (ITC) measurements for the interaction of human serum albumin with 1907, 1907-B, and GGSGSG. (E) The calculated helicity of 1907 or 1907-B in PBS or 50% TFE

biosensor experiments with surface plasmon resonance (SPR). The results showed that 1907-B exhibited >10-fold higher affinity binding to HSA (K_D = 2.54 μmol/L) than 1907 (K_D = 26.5 μmol/L) (Fig. 3C). Consistent with the above result, the ITC assay also identified that 1907-B could increase the binding affinity by ∼6-fold compared with 1907 (Fig. 3D).

Changes in structural conformation and agonistic activities on GLP-1R or GCGR between 1907 and 1907-B were also examined. The results indicated that the additional modification on 1907 could raise α-helical content, decrease the GLP-1R activity (∼44-fold), and increase GCGR activity (∼2-fold) to promote a more balanced GLP-1R/GCGR activity ratio (Fig. 3E). Based on the enhanced binding affinity between 1907-B and HSA, we needed to identify if the half-life of 1907-B could be prolonged. After 1907-B treatment for 60 h, the OGTT results showed that 1907-B still obviously improved the glucose tolerance compared with the saline group. In comparison, the 1907 and semaglutide robustly lowered glucose excursion after treatment for 48 h (Fig. 3F).

Next, we evaluated the pharmacokinetics (PK) properties of 1907-B and semaglutide by i.v. injection or s.c. injection in SD rats. As shown in Fig. 3G, following i.v. treatment, the half-lives of 1907-B and semaglutide were ∼16.8 and ∼8 h, respectively. The observed AUCs from 0 to infinity (AUCinf) of 1907-B and semaglutide were ∼8588 and ∼6194 ng h/mL, respectively. Following s.c. treatment, the half-lives of 1907-B and semaglutide were ∼20.5 and ∼7.95 h, respectively. These data in SD rats indicated that the half-life of 1907-B was prolonged to ∼2−3-fold than that of semaglutide, which is currently dosed once weekly in humans. We also assessed the PK properties of 1907-B in cynomolgus monkeys (Fig. 3H). Following s.c. treatment, the half-life of 1907-B was 84 h. These results suggest that 1907-B, an ultralong-acting peptide, has the potential to be administered once every two weeks or even less frequently.

3.5. *1907-B ameliorates chronic kidney disease in* db/db *mice in a GLP-1R and GCGR signaling-dependent manner*

To directly examine the *in vivo* efficacy of ultralong-acting 1907-B, various doses and administration frequencies of 1907-B were administrated to *db/db* mice with diabetic nephropathy. The doses administered were 60.0, 120.0, and 240.0 μg/kg/day, as well as 120.0 μg/kg/2 days. The results showed that 1907-B dramatically decreased the blood glucose and HbA1c levels in a dose-dependent manner, and the group that received 120.0 and 240.0 μg/kg/day even showed superior effects in reducing blood glucose and HbA1c levels than semaglutide (Fig. 4A and B).

Metabolic and kidney outcomes of 1907-B administration were evaluated *in vivo* using *db/db* mice with diabetic nephropathy. The mice were treated with either 1907-B (a dual GLP-1R/GCGR agonist) once every 2 days, semaglutide (a GLP-1R agonist) daily, or glucagon (a GCGR agonist) daily, all at an equivalent dose of 120.0 μg/kg for 8 weeks. The results showed that both 1907-B and semaglutide treatments led to decreased fasting glucose levels compared to the vehicle group, while glucagon alone induced higher fasting glucose levels (Supporting Information Fig. S7A). Meanwhile, the HbA1c level was significantly decreased in the 1907-B treated *db/db* mice, but not in semaglutide or glucagon-treated *db/db* mice (Fig. S7B). Interestingly, although treatment with glucagon resulted in much higher blood glucose, it still exhibited a similar effect to 1907-B and semaglutide in reducing blood urea nitrogen (BUN) and serum creatinine (CRE) (Fig. 4C and D). These effects were also confirmed by pathological results (Fig. 4E). To further explore the effects of 1907-B, semaglutide, and glucagon on DN, the RNA-seq analysis of mouse kidneys from these groups was performed. Gene Set Enrichment Analysis (GSEA) pathway enrichment results indicated that enriched pathways involved in fibrosis and inflammation were downregulated and enriched pathway involved in mitochondrial function was upregulated by 1907-B, semaglutide, and glucagon treatments compared to the control *db/db* mice (Fig. 4G, Fig. S7C and D). A heatmap based on the GSEA results indicated that genes involved in fibrosis and inflammation were downregulated and genes involved in mitochondrial function were upregulated by 1907-B, semaglutide and glucagon treatment compared with the control *db/db* mice (Fig. 4F). These data demonstrated both GLP-1R and GCGR played vital roles in DN, and 1907-B improved kidney function and inhibited kidney fibrosis *via* targeting GLP-1R and GCGR signaling.

To investigate whether the attenuation of kidney damage and fibrosis by 1907-B requires GLP-1R and GCGR signaling, we administered AAV9 vectors carrying GLP-1R or GCGR shRNA to *db/db* mice with diabetic nephropathy (GLP-1R$^{-/-}$ or GCGR$^{-/-}$). After four weeks, mice with knockdown of either GLP-1R or GCGR showed elevated fasting blood glucose levels compared to control *db/db* mice (Fig. 4H). The blood glucose-lowering effect and reduction of HbA1c levels by 1907-B were observed only in *db/db* mice lacking GCGR, not in those lacking GLP-1R (Fig. 4H and I). Interestingly, GCGR knockdown markedly reduced the potency of 1907-B in reducing BUN and SCr, while GLP-1R knockdown did not (Fig. 4J and K). Consistent with the above results, there was no effect of 1907-B treatment on glomerulosclerosis and tubulointerstitial fibrosis in GCGR knockdown *db/db* mice as observed by H&E, Masson, and Sirius Red staining (Fig. 4L). These findings further proved that 1907-B improved DN *via* targeting GLP-1R and GCGR, with GCGR playing a more important role than GLP-1R in the treatment.

3.6. *1907-B attenuates kidney fibrosis in UUO mice in a GLP-1R and GCGR signaling-dependent manner*

The UUO method has been widely used to establish animal models with obstructive nephropathy[49]. We employed this model to evaluate whether 1907-B could ameliorate CKD independently of its glucose-lowering effect. To determine the optimal dose and administration frequency of 1907-B in UUO mice, we tested various doses (60.0, 120.0, 240.0 μg/kg/day) and administration frequencies (120.0 μg/kg/2 days). The pathological results indicated that 1907-B dramatically reduced kidney inflammation and

and *in vitro* activity of 1907 or 1907-B in the GLP-1R- or GCGR-mediated CRE-Luc reporter assay. The experiments were conducted three times independently. (F) Oral glucose tolerance test (OGTT) was performed at 24, 48, and 60 h after semaglutide (120.0 μg/kg, n = 6), 1907 (120.0 μg/kg, n = 6) or 1907-B (120.0 μg/kg, n = 6) administration, respectively. The corresponding area under curves (AUC) of blood glucose levels was calculated. (G) Pharmacokinetics of semaglutide (50.0 μg/kg, n = 6) or 1907-B (50.0 μg/kg, n = 6) in SD rats. (H) Pharmacokinetics of 1907-B (25.0 μg/kg, n = 2) in cynomolgus monkeys.

fibrosis in UUO mice in a dose-dependent manner and even exhibited better efficacy than semaglutide at a very low dose (Fig. S7E).

To formally assess the effect of 1907-B on kidney fibrosis improvement *in vivo*, we treated UUO mice with equivalent doses of 1907-B (120.0 μg/kg once every 2 days), semaglutide (daily), or glucagon (daily) for 14 days. H&E, Masson, and Sirius Red staining revealed that glucagon treatment exhibited markedly fewer tubular injuries and ECM accumulation than 1907-B and semaglutide treatment (Fig. 5A). To systematically investigate how 1907-B, semaglutide and glucagon suppress UUO-induced kidney fibrosis, we performed RNA-seq analysis in the kidneys from sham and UUO-treated mice. GSEA showed that cellular signaling pathways involved in fibrosis, inflammation, and mitochondrial function were enriched (Fig. S7F). Similarly, a heatmap based on GSEA revealed that the expression of kidney genes involved in fibrosis and inflammation was significantly downregulated and the expression of kidney genes involved in mitochondrial function was upregulated by 1907-B, semaglutide, and glucagon treatment compared to the control group (Fig. 5B). However, semaglutide showed less effect in UUO-treated mice than the other two groups. We then analyzed the data in combination with the transcriptomes of DN and UUO mice, which demonstrated that nine signaling pathways were consistently influenced (Fig. 5C), and the inflammation and mitochondrial function pathways overlapped (Fig. 5D).

To further confirm the roles of GLP-1R and GCGR during the 1907-B treatment for kidney fibrosis, we tested the AAV9-GLP-1R or GCGR shRNA-treated UUO mice. H&E, Masson, and Sirius Red staining revealed that the GLP-1R or GCGR knockdown could aggravate kidney fibrosis in the UUO mice. Protection effects by 1907-B in UUO mice lacking GCGR were not observed, while 1907-B treatment in UUO mice lacking GLP-1R showed noticeable kidney protection effects, including fewer tubular injuries and ECM deposition (Fig. 5E). These findings further proved that 1907-B improved kidney fibrosis in UUO mice mainly by targeting GCGR.

3.7. 1907-B ameliorates kidney inflammation and fibrosis via IKBα-NF-κB and TGF-β1-SMAD signaling pathways

Next, we used the DN mouse model to explore the mechanisms of 1907-B treatment on CKD. According to RNA-seq analysis results, the cellular signaling pathways involved in fibrosis (such as the VEGF signaling pathway and ECM receptor interaction) were significantly downregulated after 1907-B treatments (Fig. 6A). The Western blot results also revealed that the 1907-B treatment reduced α-SMA and COL1A1 expression in *db/db* mice (Fig. 6B). Furthermore, qPCR results indicated that 1907-B treatment could suppress the genes expression related to fibrosis, such as *Serpine1*, *Desmin*, *Mmp3*, *Mmp8*, and *Mmp9*, suggesting that 1907-B treatment may not only promote ECM degradation but also decrease ECM production (Fig. 6C). It is well-known that the TGF-β/SMAD signaling pathway is pivotal in the formation of kidney fibrosis[50], we then investigated whether 1907-B could modulate the TGF-β/SMAD signaling pathway to ameliorate kidney fibrosis. As shown in Fig. 6B, the expression of pro-fibrogenic gene TGF-β1 as well as phosphorylated SMAD2/3 in *db/db* mice were down-regulated by the 1907-B treatment. Considering that fibroblast activation plays a major role in kidney interstitial fibrosis and activated fibroblasts or myofibroblasts are sources of ECM, we evaluated the impact of 1907-B on fibroblast activation using high glucose-treated GMC and mTEC cells. Similarly, the pro-fibrogenic genes such as TGF-β1 in high glucose-induced GMC and mTEC cells were also downregulated by the 1907-B treatment (Supporting Information Fig. S8A).

Inflammation is a hallmark of chronic kidney disease characterized by inflammatory cytokine production and inflammatory cell infiltration. Next, we determined the effects of 1907-B on DN-associated inflammation. RNA-seq analysis results showed the cellular signaling pathways related to inflammation (such as cytokine-cytokine receptor interaction, chemokine signaling pathway, and toll-like receptor signaling) were significantly downregulated by the 1907-B treatment (Fig. 6D). qPCR assay also showed that 1907-B treatment significantly attenuated the increase in the expression of inflammation genes (*Nos2*, *F4/80*, *Il1b*, *Il6*, Ccl2, and *Ccl4*) in *db/db* mice (Fig. 6E). The anti-inflammatory effect of the 1907-B treatment was also revealed by the reduction in inflammatory cell infiltration from the kidneys, as verified by immunohistochemistry staining for the macrophage marker CD68 (Fig. 6F). Similarly, the Western blot results also identified that the 1907-B treatment could significantly decrease the expression of the inflammation genes (CD68, TNF-α, and IL-1β) (Fig. 6G). NF-κB signaling is activated in *db/db* mice with DN. The Western blot results exhibited that the protein levels of p-IKBα and p-P65 were significantly decreased by the 1907-B treatment (Fig. 6G). Consistent with the results in *db/db* mice, the Western blot results in high glucose-induced GMC and mTEC cells also showed that the protein levels of p-IKBα and p-P65 were remarkably reduced by 1907-B treatment, whereas those of IKBα were increased by 1907-B, suggesting that 1907-B suppresses the activation of NF-κB signaling and related inflammation (Fig. S8B).

3.8. 1907-B improves mitochondrial function and inhibits oxidative stress via PKA signaling

Mitochondrial dysfunction has been implicated in diabetic nephropathy pathogenesis. RNA-Seq data showed that the 1907-B treatment affected diverse signaling pathways involved in metabolism, such as butanoate metabolism, citrate cycle TCA cycle, peroxisome, and oxidative phosphorylation (Fig. 7A). Oxidative stress was detected by the determination of levels of SOD, CAT, HO-1 and the activity of GSH, CAT, and T-SOD in kidney tissues. These data showed the 1907-B treatment could remarkably ameliorate levels and activity of these antioxidants in *db/db* mice (Fig. 7B and C). In addition, we also examined the levels of 4-HNE and NOX4 in *db/db* mice after 1907-B treatment using immunofluorescence staining and the results showed that 1907-B treatment significantly reduced the contents of 4-HNE and NOX4 in *db/db* mice (Fig. 7D). Similar results were also observed by Western blot detection in *db/db* mice or high glucose-induced GMC and mTEC cells after 1907-B treatment (Fig. 7E and Fig. S8C).

Furthermore, we evaluated the effect of 1907-B on the improvement of mitochondrial function. qPCR analysis showed that 1907-B could increase the expression of genes related to mitochondrial function, such as *Ppargc1a*, *Ppargc1b*, *Uqcrc1*, and *Gpx1*. Similarly, the Western blot detection also identified that 1907-B could increase the expression of proteins related to mitochondrial function, such as PGC-1α and PGC-1β in *db/db* mice or high glucose-induced GMC and mTEC cells after 1907-B treatment (Fig. 7F and Fig. S8D). A decreased number of green-labeled mitochondria was observed in high glucose-treated cells in

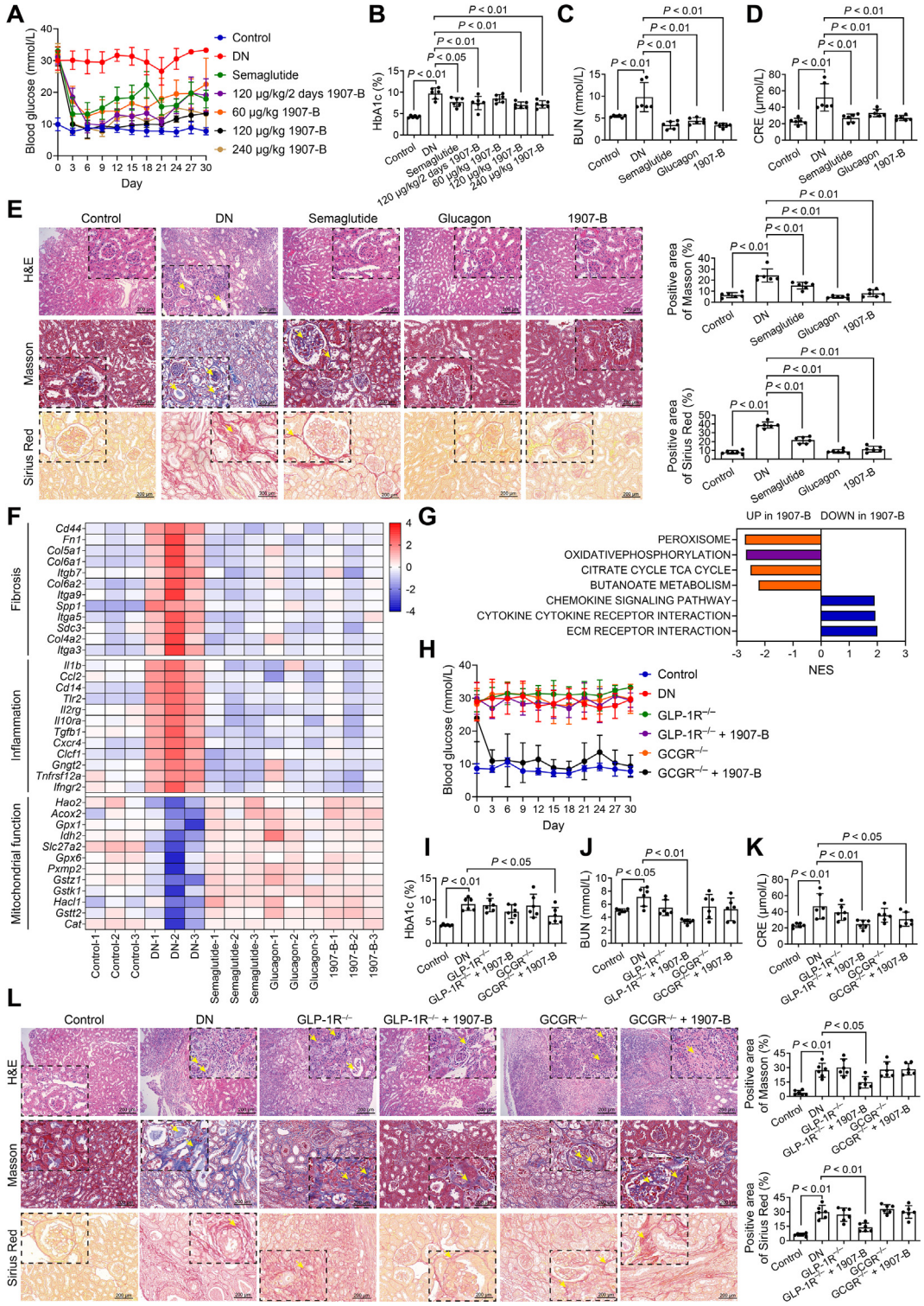

Figure 4 1907-B improves kidney fibrosis in diabetic *db/db* mice in a GLP-1R and GCGR signaling-dependent manner. (A) The fasting blood glucose and (B) glycated hemoglobin of *db/db* mice after 4-week administration with semaglutide or 1907-B. (C) Blood urea nitrogen and (D) serum creatinine levels of *db/db* mice treated with semaglutide (120.0 μg/kg/day, $n = 6$), glucagon (120.0 μg/kg/day, $n = 6$), or 1907-B (120.0 μg/kg/2 days, $n = 6$) at study endpoint. (E) Representative images of H&E, Masson, and Sirius Red staining on kidneys from *db/db* mice at indicated groups ($n = 6$/group) and bar graphs of positive area, respectively. Arrows indicate positive staining. (F) Heatmap of fibrosis-, inflammation-, and mitochondrial function-related gene expression profiles based on the RNA-Seq dataset. (G) GSEA of pathways related to fibrosis, inflammation and mitochondrial function in *db/db* mice treated with 1907-B (120.0 μg/kg/2 days, $n = 6$). (H) The fasting blood glucose and (I) glycated hemoglobin of GLP-1R$^{-/-}$ or GCGR$^{-/-}$ *db/db* mice after 4-week administration with 1907-B (120.0 μg/kg/2 days, $n = 6$). (J) Blood urea nitrogen and (K) serum creatinine levels of GLP-1R$^{-/-}$ or GCGR$^{-/-}$ *db/db* mice treated with 1907-B (120.0 μg/kg/2 days, $n = 6$) at study endpoint. (L) Representative images of H&E, Masson, and Sirius Red staining on kidneys from GLP-1R$^{-/-}$ or GCGR$^{-/-}$ *db/db* mice at indicated groups ($n = 6$/group) and bar graphs of positive area, respectively. Arrows indicate positive staining.

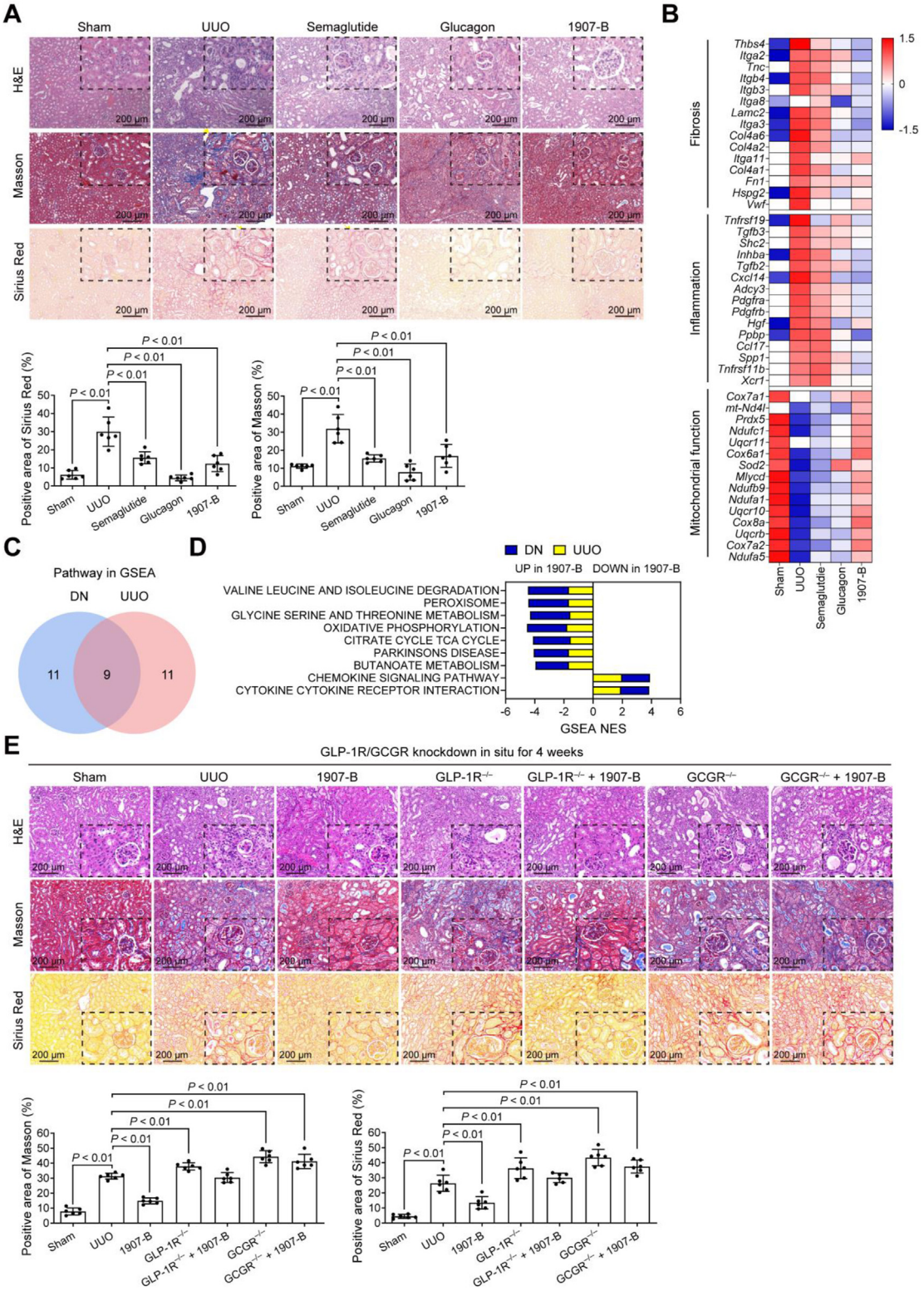

Figure 5 1907-B improves kidney fibrosis in UUO mice in a GLP-1R and GCGR signaling-dependent manner. (A) Representative images of H&E, Masson and Sirius Red staining in kidneys from UUO mice treated with semaglutide (120.0 μg/kg/day, $n = 6$), glucagon (120.0 μg/kg/day, $n = 6$) or 1907-B (120.0 μg/kg/2 days, $n = 6$) and bar graphs of positive area, respectively. Arrows indicate positive staining. (B) Heatmap of fibrosis-, inflammation- and mitochondrial function-related gene expression profiles based on the RNA-Seq dataset. (C−D) Venn diagram and the corresponding scores of the intersecting pathways based on the transcriptomic data from *db/db* mouse and UUO mouse kidney samples. (E) Representative images of H&E, Masson, and Sirius Red staining of kidneys from GLP-1R$^{-/-}$ or GCGR$^{-/-}$ UUO mice treated with 1907-B (120.0 μg/kg/2 days, $n = 6$) and bar graphs of positive area, respectively.

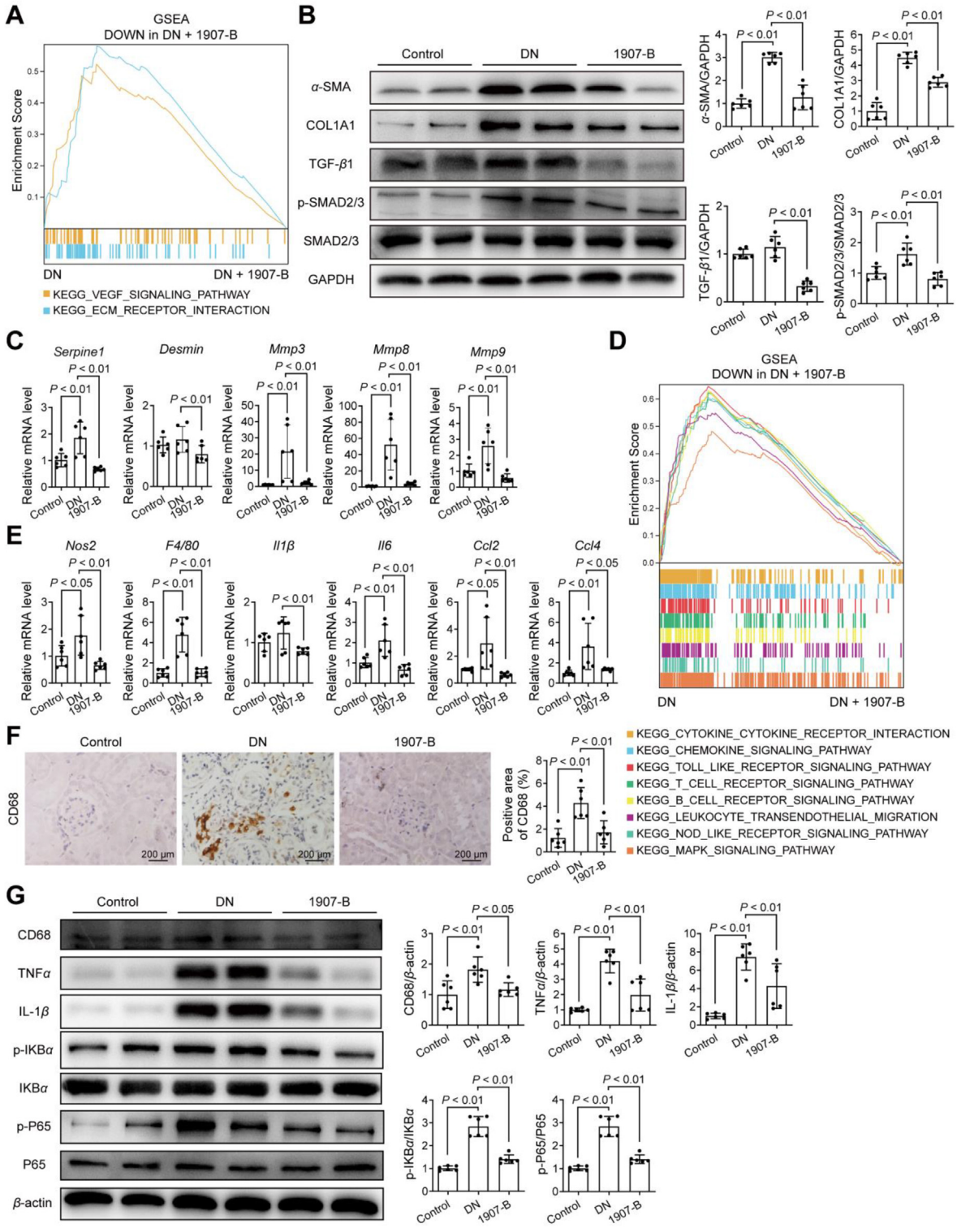

Figure 6 1907-B ameliorates kidney inflammation and fibrosis *via* IKBα-NF-κB and TGF-β1-Smad signaling pathways. (A) GSEA pathway enrichment analysis of pathways related to fibrosis. (B) The expression levels of key proteins including α-SMA, COL1A1, TGF-β1, and p-SMAD2/3/SMAD2/3 in the kidneys of the indicated groups. Here and hereafter, unless otherwise indicated, the quantifications of protein expression level were performed using three independent Western blotting experiments. (C) The mRNA levels of *Serpine1*, *Desmin*, *Mmp3*, *Mmp8*, and *Mmp9* were measured in the kidney samples of the indicated groups ($n = 6$/group). (D) GSEA pathway enrichment analysis of pathways related to inflammation. (E) The mRNA levels of *Nos2*, *F4/80*, *Il1b*, *Il6*, *Ccl2*, and *Ccl4* were measured in the kidney samples of the indicated groups ($n = 6$/group). (F) Representative images of immunohistochemistry staining of CD68 on kidneys from *db/db* mice at indicated groups ($n = 6$/group) and bar graphs of positive area, respectively. (G) The expression level of key protein CD68, TNFα, IL-1β, p-IKBα/IKBα, and p-P65/P65 in the kidneys of the indicated groups.

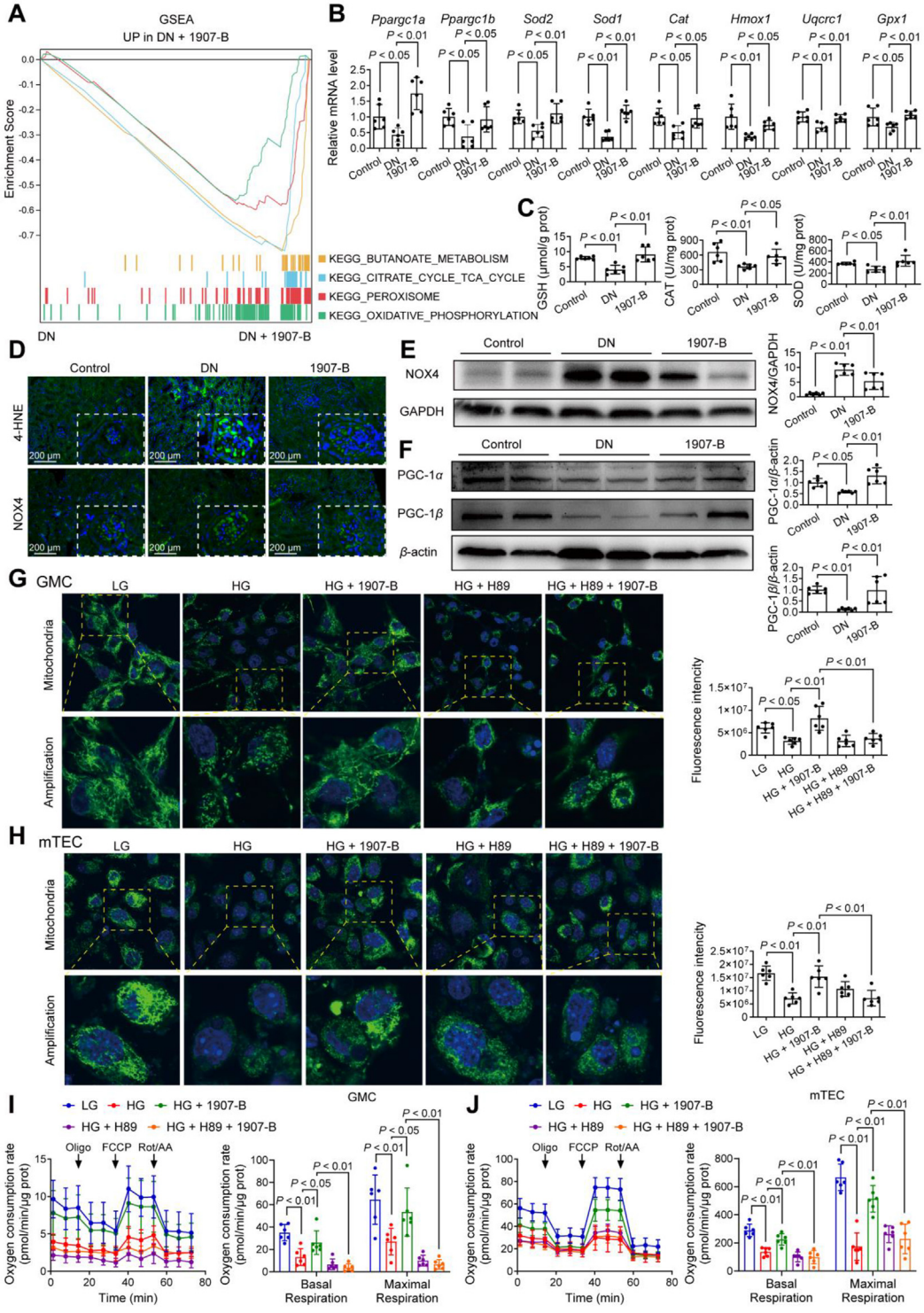

Figure 7 1907-B improves mitochondrial function and inhibits oxidative stress. (A) GSEA pathway enrichment analysis of pathways related to mitochondrial function. (B) The mRNA levels of *Ppargc1a*, *Ppargc1b*, *Sod1*, *Sod2*, *Cat*, *Hmox1*, *Uqcrc1*, and *Gpx1* were measured in the kidney samples of the indicated groups ($n = 6$/group). (C) The GSH content and activity of antioxidant stress related enzyme CAT and SOD in the kidney samples of the indicated groups ($n = 6$/group). (D) Representative images of fluorescence staining of 4-HNE and NOX4 in kidneys from *db/db* mice in the indicated groups ($n = 6$/group). (E–F) The expression levels of key proteins including NOX4, PGC-1α, and PGC-1β in the kidneys of the indicated groups. (G–H) Representative live cell confocal microscopy images showing GMC cells and mTEC cells of the indicated groups stained with Mito Tracker following treatment with 1907-B (20.0 μmol/L), both with and without H89 (5.0 μmol/L). (I–J) OCR during mitochondrial stress test of GMC cells and mTEC cells under high glucose following treatment with 1907-B (20.0 μmol/L), both with and without H89 (5.0 μmol/L). The figures shown are representative of three independent experiments.

comparison to the control (Fig. 7G and H). In contrast, 1907-B could significantly recover the mitochondrial damage induced by high glucose. Mitochondrial fission is often used as the determinant of mitochondrial function[51]. The mitochondrial length was examined to quantify mitochondrial fission. We observed the morphological changes in mitochondria under high glucose treatment, and the mitochondrial length was significantly reduced compared with the control. In contrast, 1907-B treated cells showed predominantly elongated forms of mitochondria despite high glucose treatment. However, H89 (a PKA inhibitor) could abolish the improvement in mitochondrial maintenance by 1907-B.

Next, we used the oxygen-consumption rate (OCR) assay to evaluate mitochondrial respiratory function. GMC and mTEC cells exposed to the medium containing high glucose displayed notably reduced basal and maximal respiration rates compared with that in low glucose medium (Fig. 7I and J). Treatment with 1907-B restored basal and maximal respiratory rates in high glucose-induced GMC and mTEC cells. When PKA was inhibited, 1907-B was unable to increase OCR in GMC and mTEC cells, which indicated that the improved mitochondrial function was mediated by the PKA signaling. These findings indicated that 1907-B could decrease oxidative stress and ameliorate mitochondrial function to further improve chronic kidney injury *via* PKA signaling.

4. Discussion

Several studies indicate that mitochondrial dysfunction, oxidative stress, inflammation, apoptosis and ECM deposition are implicated in the progression of kidney diseases[52]. Therefore, strategies for CKD treatment should target the key factors involved in prominent pathogenic pathways in this condition to ultimately inhibit multiple pathological features in a simultaneous manner[5,53].

In this study, we first identified GLP-1R and GCGR as key regulators of CKD. Their expression was correlated with the severity of chronic kidney injury in two mouse models of CKD. Specifically, downregulation of GLP-1R and GCGR in the kidneys significantly aggravated diabetic nephropathy in *db/db* mice, concomitant with increased kidney fibrosis, inflammation, and impaired mitochondrial function. Similarly, GLP-1R and GCGR knockdown also exacerbated kidney fibrosis in UUO mice. Considering the hypoglycemic effect and the antioxidant effect of GLP-1 as well as the effect of glucagon on improving mitochondrial function, we speculate that concurrent agonism of GLP-1R and GCGR could alleviate CKD by preventing hyperglycemia and attenuating mitochondrial dysfunction.

Many attempts are currently being undertaken to develop GLP-1R/GCGR co-agonists, and some of these medications have been successfully applied to the treatment of NASH, obesity, and diabetes. However, the effect of GLP-1R/GCGR co-agonists on CKD treatment remains uncertain[54]. In this study, we engineered several GLP-1R/GCGR co-agonist analogs and identified 1907-B as a safe, highly effective, ultralong-acting basal contender with strong and reversible albumin binding, proteolytic stability, and high GLP-1/GCG receptor affinity. We originally introduced the concept of “double-site recognition” *via* octadecanedioic (C18) and the glycine/serine-based linker (GGSGSG) binding to albumin to optimize drug release. *In vivo*, pharmacokinetic data in SD rats and cynomolgus monkeys revealed that the half-life of 1907-B was prolonged ∼2−3-fold than semaglutide, allowing for a dosing frequency of once every two weeks or even less frequently.

Next, the efficacy of 1907-B in improving DN was confirmed in 20-week-old diabetic *db/db* mice. Indeed, 1907-B significantly reduced high blood glucose levels and ameliorated kidney injury. Interestingly, both GLP-1R-specific agonist semaglutide and GCGR-specific agonist glucagon effectively inhibited kidney damage, respectively. According to Yamada et al.[24], GLP-1R signaling has a crucial role in the development and progression of DN, and GLP-1R agonists such as exendin-4 and liraglutide attenuated diabetic kidney injury through the protection of glomerular endothelial cells, reduction of kidney oxidative stress, and suppression of kidney inflammatory cytokines, which could explain the pharmacologic action of semaglutide. On the other hand, although glucagon caused high blood glucose levels, it significantly inhibited kidney injury *via* modulating mitochondrial turnover, which indicated that mitochondrial function played a vital role in the process of DN and targeting glycolysis alone may not be a wise choice for DN treatment. Consistent with the selective pharmacological activation studies reported here, the improvement effect of 1907-B on diabetic kidney damage was significantly affected in *db/db* mice with down-regulated GLP-1R or GCGR expression. Moreover, it should be noted that the 1907-B treatment exhibited partial anti-diabetic nephropathy effects in *db/db* mice lacking GLP-1R, but not in *db/db* mice lacking GCGR. Taken together, GCGR signaling has a more important role than GLP-1R signaling during 1907-B treatment for DN.

To eliminate the interference of the glucose-lowering effect of 1907-B and evaluate if the 1907-B could improve kidney fibrosis independent on affecting blood glucose changes, we performed the UUO surgery to build the kidney fibrosis model and further investigated its kidney phenotype under 1907-B treatment. Our results demonstrated that the 1907-B treatment exhibited fewer tubular injuries and ECM deposition. Interestingly, glucagon had the most significant effect in improving kidney fibrosis among these three treatment groups. Similarly, GLP-1R or GCGR knockdown assay also identified GCGR as a critical role in the treatment of 1907-B for kidney fibrosis.

Mechanistically, substantial data in this study have indicated that 1907-B could reduce kidney injury *via* multiple mechanisms. First, 1907-B treatment attenuates kidney oxidative stress and increases the expression of antioxidant factors *via* GLP-1 signaling. On the other hand, 1907-B could also improve mitochondrial turnover *via* glucagon signaling. In short, both of them can further improve mitochondrial function. Furthermore, 1907-B protects the kidney against inflammation *via* the NF-κB pathway and kidney fibrosis *via* the TGF-β-SMAD pathway. Finally, our data reveal that the treatment of 1907-B improves kidney oxidative stress, inflammation, kidney injury and fibrosis *via* targeting GLP-1R and GCGR, as summarized in Fig. 8.

Prior to clinical trials on human subjects, pre-clinical evaluation of drugs is a crucial process that involves laboratory and animal studies to determine the safety, efficacy, and pharmacokinetic properties of a drug candidate. In this study, the drug target profile screening assays confirmed that 1907-B was highly specific and did not respond to other receptors, minimizing the risk of unwanted side effects (Supporting Information Table S10). The safety pharmacology and toxicology studies of 1907-B evaluation were also systematically performed in SD rats and cynomolgus monkeys and 1907-B had negligible adverse effects and did not elicit a significant immune response (data not shown). In addition to the results described above, 1907-B treatment was also administrated to Zucker diabetic fatty (ZDF) rats, an animal model for the study of type 2 diabetes, for 18-week long-term

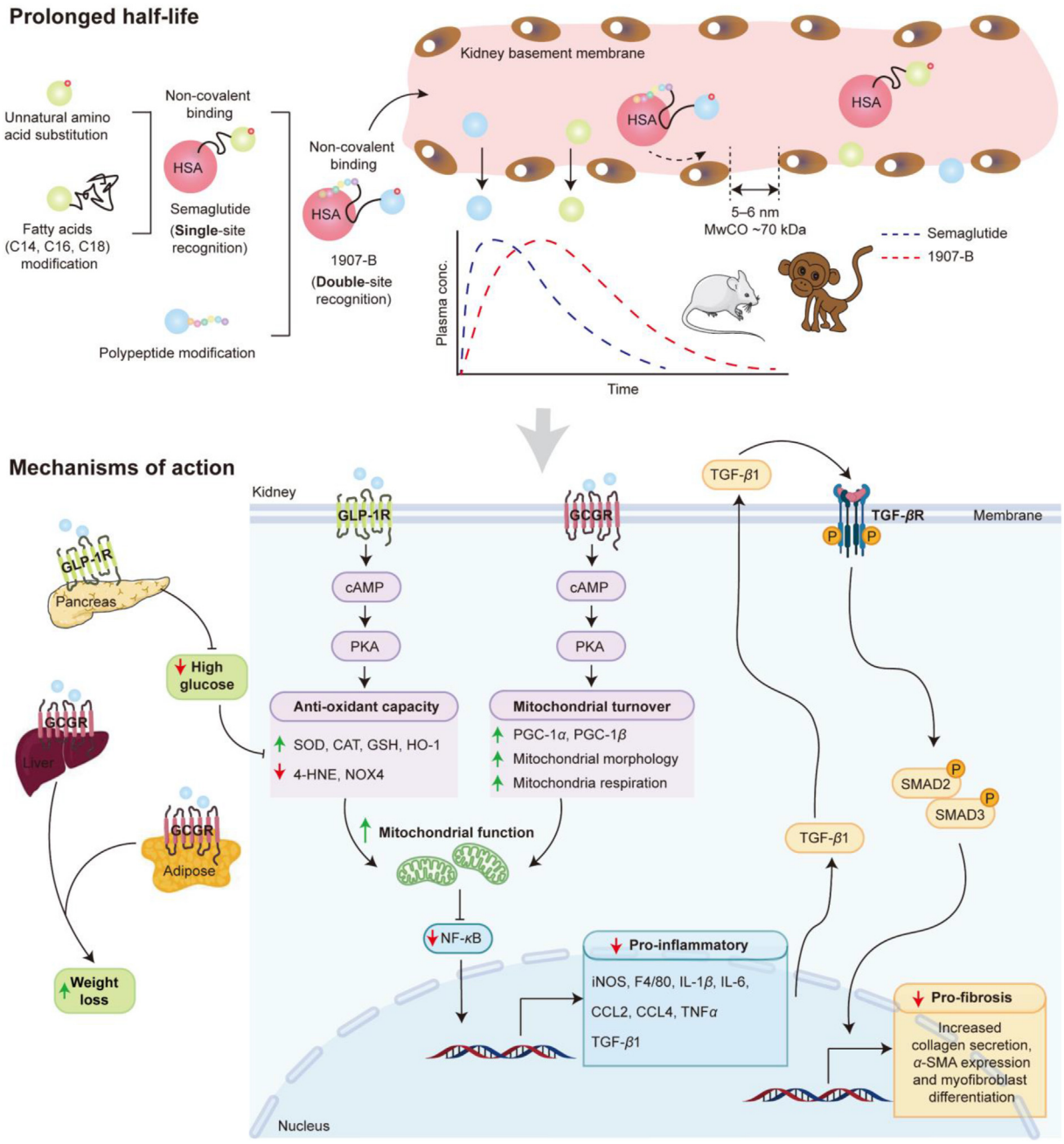

Figure 8 Summary of the design of ultralong-acting GLP-1 and glucagon co-agonist 1907-B and its mechanisms of action on target organs. Compared with semaglutide, 1907-B exhibits a longer half-life due to the introduction of C18 and "GGSGSG" in the side chain of Lys at position 10 of 1907. Mechanistically, 1907-B could act on the GCGR in the liver and adipose tissue to reduce body weight. Moreover, the GLP-1R agonist activity at pancreatic β-cells enhances insulin secretion to reduce blood glucose. In the kidney, GLP-1R signaling could increase anti-oxidant capacity and lead to lower levels of oxidative stress; and GCGR signaling could improve mitochondrial maintenance. Moreover, the activation of GLP-1R and GCGR signaling could further reduce inflammation *via* the NF-κB pathway and ameliorate kidney fibrosis *via* the TGF-β-SMAD pathway.

dosing trials to establish the safety and efficacy of 1907-B over a prolonged period. Following 18-week treatment, 1907-B significantly improved diabetes and diabetic nephropathy accompanied by reduced fasting blood glucose levels and HbA1c level, as well as decreased 24-h urine microalbumin protein and urine albumin-to-creatinine ratio (ACR) levels compared to diabetic controls (Supporting Information Fig. S12 and Tables S6−S9). Moreover, we further evaluated the genotoxicity, including the Salmonella/microsome mutagenicity assay (Ames test), The Chromosome Aberration Assay (CAA), and the Bone Marrow Micronucleus Test (BMMT), and all of them exhibited negative results (data not shown). The effect of 1907-B with 2 mg/mL on hemolysis was investigated *in vitro* and the test results showed no hemolysis and/or erythrocyte coagulation, which suggested that 1907-B was negative for hemolysis *in vitro* (data not shown). Currently, preclinical studies of 1907-B in diabetic nephropathy have been

completed, and it has received clinical trial approval to enter phase I clinical trials (approved No. 2022LP01773) in China. Future results will provide more information on its clinical potential. To summarize, this study has highlighted the significant contribution of GLP1-R/GCGR signaling to the development and progression of CKD and has presented a potential co-agonist that has shown effectiveness in mitigating CKD, thus paving the way for promising therapeutic development in this area.

Acknowledgments

We appreciate the financial support from the National Natural Science Foundation of China (No. 82273761 and No. 81871257), the Medical Innovation and Development Project of Lanzhou University (lzuyxcx-2022-156, China), the Undergraduate Teaching Quality Engineering Project of Sun Yat-sen University [2021] 93 and the Guangdong Provincial Key Laboratory of Construction Foundation (2023B1212060022, China).

Author contributions

Xianxing Jiang, Guodong Chen, and Rui Wang conceived and designed the research and supervised the studies. Qian Zhao, Jiale Dong, and Han Liu performed the experiments and analyzed data. Nazi Song and Hongjiao Xu supported the peptide synthesis and purification. Hui Chen and Shuyin Ye performed the cell experiments and the acquisition of data. Huan Yu, Qi Liu, and Yuyi Li performed the animal models. Zhiteng Luo construct the three-dimensional model of the 1907/GLP-1R complex. Shuangjin Yu, Longhui Qiu, and Yu Li performed and collected the data about pre-clinical studies. Xianxing Jiang analyzed the data and wrote the manuscript.

Conflicts of interest

The authors declare competing financial interests: details are available in the online version of the paper.

Appendix A. Supporting information

Supporting data to this article can be found online at https://doi.org/10.1016/j.apsb.2023.11.020.

References

1. Zhao YY. Chronic kidney disease: biomarker diagnosis to therapeutic targets. *Clin Chim Acta* 2019;**499**:54−63.
2. Ferenbach DA, Bonventre JV. Acute kidney injury and chronic kidney disease: from the laboratory to the clinic. *Nephrol Ther* 2016;**12**: S41−8.
3. Nahas A, Muchaneta-Kubara EC, Essaway M, Soylemezoglu O. Renal fibrosis: insights into pathogenesis and treatment. *Int J Biochem Cell Biol* 1997;**29**:55−62.
4. Liu Y, Wang Y, Ding W, Wang Y. Mito-TEMPO alleviates renal fibrosis by reducing inflammation, mitochondrial dysfunction, and endoplasmic reticulum stress. *Oxid Med Cell Longev* 2018;**2018**: 5828120.
5. Nastase MV, Zeng-Brouwers J, Wygrecka M, Schaefer L. Targeting renal fibrosis: mechanisms and drug delivery systems. *Adv Drug Deliv Rev* 2018;**129**:295−307.
6. Delles C, Vanholder R. Chronic kidney disease. *Clin Sci* 2017;**131**: 225−6.
7. D Uni A, Liakopoulos V, Roumeliotis S, Peschos D, Dounousi E. Oxidative stress in the pathogenesis and evolution of chronic kidney disease: untangling ariadne's Thread. *Int J Mol Sci* 2019;**20**:3711.
8. Ruiz S, Pergola PE, Zager RA, Vaziri ND. Targeting the transcription factor Nrf2 to ameliorate oxidative stress and inflammation in chronic kidney disease. *Kidney Int* 2013;**83**:1029−41.
9. Hu R, Wan MQ, Liu LY, You HY, Wu XH, Liu YY, et al. Calycosin inhibited autophagy and oxidative stress in chronic kidney disease skeletal muscle atrophy by regulating AMPK/SKP2/CARM1 signalling pathway. *J Cell Mol Med* 2020;**24**:11084−99.
10. Sureshbabu A, Ryter SW, Choi ME. Oxidative stress and autophagy: crucial modulators of kidney injury. *Redox Biol* 2015;**4**:208−14.
11. Rapa SF, Iorio B, Campiglia P, Heidland A, Marzocco S. Inflammation and oxidative stress in chronic kidney disease—potential therapeutic role of minerals, vitamins and plant-derived metabolites. *Int J Mol Sci* 2020;**21**:263.
12. Moreno JA, Gomez-Guerrero C, Mas S, Sanz AB, Lorenzo O, Ruiz-Ortega M, et al. Targeting inflammation in diabetic nephropathy: a tale of hope. *Expert Opin Investig Drugs* 2018;**27**:917−30.
13. Czaya B, Faul C. FGF23 and inflammation-a vicious coalition in CKD. *Kidney Int* 2019;**96**:813−5.
14. Chen H, Fang Y, Wu J, Chen H, Zou Z, Zhang X, et al. RIPK3-MLKL-mediated necroinflammation contributes to AKI progression to CKD. *Cell Death Dis* 2018;**9**:878.
15. Nogueira A, Pires MJ, Oliveira PA. Pathophysiological mechanisms of renal fibrosis: a review of animal models and therapeutic strategies. *In Vivo* 2017;**31**:1−22.
16. Bhargava P, Schnellmann RG. Mitochondrial energetics in the kidney. *Nat Rev Nephrol* 2017;**13**:629−46.
17. Pieczenik SR, Neustadt J. Mitochondrial dysfunction and molecular pathways of disease. *Exp Mol Pathol* 2007;**83**:84−92.
18. Che R, Yuan Y, Huang S, Zhang A. Mitochondrial dysfunction in the pathophysiology of renal diseases. *Am J Physiol Ren Physiol* 2014; **306**:367−78.
19. Elmarakby AA, Sullivan JC. Relationship between oxidative stress and inflammatory cytokines in diabetic nephropathy. *Cardiovasc Ther* 2012;**30**:49−59.
20. Bai M, Chen H, Ding D, Song R, Lin J, Zhang Y, et al. MicroRNA-214 promotes chronic kidney disease by disrupting mitochondrial oxidative phosphorylation. *Kidney Int* 2019;**95**:1389−404.
21. Small DM, Coombes JS, Bennett N, Johnson DW, Gobe GC. Oxidative stress, anti-oxidant therapies and chronic kidney disease. *Nephrology* 2012;**17**:311−21.
22. Duann P, Lin PH. Mitochondria damage and kidney disease. *Adv Exp Med Biol* 2017;**982**:529−51.
23. Jha JC, Gray SP, Barit D, Okabe J, El-Osta A, Namikoshi T, et al. Genetic targeting or pharmacologic inhibition of NADPH oxidase nox4 provides renoprotection in long-term diabetic nephropathy. *J Am Soc Nephrol* 2014;**25**:1237−54.
24. Fujita H, Morii T, Fujishima H, Sato T, Shimizu T, Hosoba M, et al. The protective roles of GLP-1R signaling in diabetic nephropathy: possible mechanism and therapeutic potential. *Kidney Int* 2014;**85**: 579−89.
25. Drucker DJ. Mechanisms of action and therapeutic application of glucagon-like peptide-1. *Cell Metab* 2018;**27**:740−56.
26. Farah LX, Valentini V, Pessoa TD, Malnic G, McDonough AA, Girardi AC. The physiological role of glucagon-like peptide-1 in the regulation of renal function. *Am J Physiol Ren Physiol* 2016;**310**: F123−7.
27. Thomas MC. The potential and pitfalls of GLP-1 receptor agonists for renal protection in type 2 diabetes. *Diabetes Metab* 2017;**43**:2S20−7.
28. Bendicho-Lavilla C, Seoane-Viaño I, Otero-Espinar FJ, Luzardo-Álvarez A. Fighting type 2 diabetes: formulation strategies for peptide-based therapeutics. *Acta Pharm Sin B* 2022;**12**:621−36.
29. Boland ML, Laker RC, Mather K, Nawrocki A, Oldham S, Boland BB, et al. Resolution of NASH and hepatic fibrosis by the GLP-1R and GCGR dual-agonist cotadutide *via* modulating mitochondrial function and lipogenesis. *Nat Metab* 2020;**2**:413−31.

30. Song N, Xu H, Liu J, Zhao Q, Chen H, Yan Z, et al. Design of a highly potent GLP-1R and GCGR dual-agonist for recovering hepatic fibrosis. *Acta Pharm Sin B* 2022;**12**:2443−61.
31. Day JW, Ottaway N, Patterson JT, Gelfanov V, Smiley D, Gidda J, et al. A new glucagon and GLP-1 co-agonist eliminates obesity in rodents. *Nat Chem Biol* 2009;**5**:749−57.
32. Gault VA, Bhat VK, Irwin N, Flatt PR. A novel glucagon-like peptide-1 (GLP-1)/glucagon hybrid peptide with triple-acting agonist activity at glucose-dependent insulinotropic polypeptide, GLP-1, and glucagon receptors and therapeutic potential in high fat-fed mice. *J Biol Chem* 2013;**288**:35581−91.
33. Kannt A, Madsen AN, Kammermeier C, Elvert R, Klockener T, Bossart M, et al. Incretin combination therapy for the treatment of non-alcoholic steatohepatitis. *Diabetes Obes Metab* 2020;**22**:1328−38.
34. Clemmensen CCJ, Finan B, Sullivan L, Fischer K, Küchler D, Sehrer L, et al. GLP-1/glucagon coagonism restores leptin responsiveness in obese mice chronically maintained on an obesogenic diet. *Diabetes Obes Metab* 2014;**63**:1422−7.
35. Pocai A, Carrington PE, Adams JR, Wright M, Eiermann G, Zhu L, et al. Glucagon-like peptide 1/glucagon receptor dual agonism reverses obesity in mice. *Diabetes* 2009;**58**:2258−66.
36. Day JW, Gelfanov V, Smiley D, Carrington PE, Eiermann G, Chicchi G, et al. Optimization of co-agonism at GLP-1 and glucagon receptors to safely maximize weight reduction in DIO-rodents. *Biopolymers* 2012;**98**:443−50.
37. Finan BMT, Ottaway N, Müller TD, Habegger KM, Heppner KM, Kirchner H, et al. Unimolecular dual incretins maximize metabolic benefits in rodents, monkeys, and humans. *Sci Transl Med* 2013;**5**. 209ra151.
38. Finan B, Yang B, Ottaway N, Smiley DL, Ma T, Clemmensen C, et al. A rationally designed monomeric peptide triagonist corrects obesity and diabetes in rodents. *Nat Med* 2015;**21**:27−36.
39. Pocai A. Action and therapeutic potential of oxyntomodulin. *Mol Metab* 2014;**3**:241−51.
40. Philip A, Parker VE, Michael S, Posch MG, Tim H, Leona PM, et al. MEDI0382, a GLP-1 and glucagon receptor dual agonist, in obese or overweight patients with type 2 diabetes: a randomised, controlled, double-blind, ascending dose and phase 2a study. *Lancet* 2018;**391**:2607−18.
41. Glessner M. American diabetes Association−75th scientific Sessions (June 5−9, 2015−Boston, MA, USA). *Drugs Today* 2015;**51**:383−6.
42. Schievenbusch SSI, Scheffler M, Nischt R, Coutelle O, Hösel M, Hallek M, et al. Combined paracrine and endocrine AAV9 mediated expression of hepatocyte growth factor for the treatment of renal fibrosis. *Mol Ther* 2010;**18**:1302−9.
43. Rocca CJ, Ur SN, Harrison F, Cherqui S. rAAV9 combined with renal vein injection is optimal for kidney-targeted gene delivery: conclusion of a comparative study. *Gene Ther* 2014;**21**:618−28.
44. Jiang N, Jing L, Li Q, Su S, Yang Q, Zhou F, et al. Design of novel Xenopus GLP-1-based dual glucagon-like peptide 1 (GLP-1)/glucagon receptor agonists. *Eur J Med Chem* 2021;**212**:113118.
45. Yap MKK, Misuan N. Exendin-4 from heloderma suspectum venom: from discovery to its latest application as type II diabetes combatant. *Basic Clin Pharmacol Toxicol* 2019;**124**:513−27.
46. Ma T, Huo S, Xu B, Li F, Wang P, Liu Y, et al. A novel long-acting oxyntomodulin analogue eliminates diabetes and obesity in mice. *Eur J Med Chem* 2020;**203**:112496.
47. Lee ES, Youn YS. Albumin-based potential drugs: focus on half-life extension and nanoparticle preparation. *J Pharm Investig* 2016;**46**:305−15.
48. Li A, Peng R, Sun Y, Liu H, Peng H, Zhang Z. LincRNA 1700020I14Rik alleviates cell proliferation and fibrosis in diabetic nephropathy *via* miR-34a-5p/Sirt1/HIF-1α signaling. *Cell Death Dis* 2018;**9**:461.
49. Bai Y, Wang W, Yin P, Gao J, Na L, Sun Y, et al. Ruxolitinib alleviates renal interstitial fibrosis in UUO mice. *Int J Biol Sci* 2020;**16**:194−203.
50. Zhao X, Kwan JYY, Yip K, Liu PP, Liu FF. Targeting metabolic dysregulation for fibrosis therapy. *Nat Rev Drug Discov* 2020;**19**:57−75.
51. Du K, Ramachandran A, Jaeschke H. Oxidative stress during acetaminophen hepatotoxicity: sources, pathophysiological role and therapeutic potential. *Redox Biol* 2013;**10**:148−56.
52. Wei D, Guo H, Xu C, Wang B, Feng D. Mitochondrial reactive oxygen species-mediated NLRP3 inflammasome activation contributes to aldosterone-induced renal tubular cells injury. *Oncotarget* 2016;**7**:17479−91.
53. Bhattacharjee N, Barma S, Konwar N, Dewanjee S, Manna P. Mechanistic insight of diabetic nephropathy and its pharmacotherapeutic targets: an update. *Eur J Pharmacol* 2016;**791**:8−24.
54. Cui J, Shang A, Wang W, Chen W. Rational design of a GLP-1/GIP/Gcg receptor triagonist to correct hyperglycemia, obesity and diabetic nephropathy in rodent animals. *Life Sci* 2020;**260**:118339.